Galactose 6-sulfate collision induced dissociation using QM+MM chemical dynamics simulations and ESI-MS/MS experiments.

Daniel Ortiz, Jean-Yves Salpin, Kihyung Song, Riccardo Spezia

Galactose 6-sulfate collision induced dissociation from QM+MM chemical dynamics simulations and ESI-MS/MS experiments.

*Daniel Ortiz,[1,2] Jean-Yves Salpin[*1,2] Kihyung Song[3] and Riccardo Spezia[*1,2]*

1) Université d'Evry Val d'Essonne - Laboratoire Analyse et Modélisation pour la Biologie et l'Environnement, Boulevard François Mitterrand, 91025 Evry Cedex (France).
2) CNRS- UMR 8587.
3) Department of Chemistry, Korea National University of Education, Chungbuk, Republic of Korea

Correspondence to:riccardo.spezia@univ-evry.fr; jean-yves.salpin@univ-evry.fr

ABSTRACT

This work combines theoretical and experimental approaches to explore the fragmentation mechanisms occurring during the collision-induced dissociation (CID) of Galactose-6-Sulfate (Gal-6S). This compound is a building block of sulfated sugars and its study can shed light on fragmentation mechanisms occurring for other systems. In particular, to understand in detail the fragmentation mechanisms at the molecular level, we have coupled mixed quantum/classical (QM+MM) direct chemical dynamics simulations with tandem mass spectrometry (MS/MS) experiments. Our results, on one hand, are in a good agreement with the "charge-remote" picture, which is usually proposed in the literature as fragmentation mechanism to account for the formation of many fragment ions. On the other hand, to reproduce some of the fragments ions obtained during our experiments, alternate dissociation pathways are proposed.

Keywords: Collision-induced dissociation, Chemical dynamics, QM/MM chemical dynamics, Electrospray, Glycosaminoglycans, Structural analysis, Fragmentation pattern, charge-remote.

1. INTRODUCTION

Carbohydrates are the most abundant biomolecules found in nature. They playing important roles in many different biological processes.[1] Nevertheless, their structural characterization remains a critical challenge in glycobiology.[2] A complete structural description of carbohydrates implies notably exact mass measurement, sites and anomeric configuration of the glycosidic linkages, and location of functional groups. In this context, mass spectrometry, through the use of collision induced dissociation (CID) combined with atmospheric pressure ionization techniques, is a very powerful method for their characterization. However, MS/MS spectra of glycans are often more complex than those of peptides and proteins. In the case of sulfated saccharides, in particular, locating the position of sulfate groups can be particularly difficult since these are easily eliminated either in source or during CID processes, resulting in a loss of information. Nowadays, soft ionization techniques such as MALDI[3, 4], DESI[5] and ESI[6, 7] can be used to successfully produce abundant negative ions without losing sulfate groups. Concerning structural characterization, several groups have examined the effect onto the MS/MS spectra of both the number and position of the sulfate groups, and of the charge of the precursor ion. It has been shown that the product ion pattern strongly depends on the charge state of the precursor ion,[8-10] and that for highly sulfated oligosaccharides several fragmentation processes (glycosidic bond cleavages and losses of H_2SO_4 equivalents) compete, resulting in very complex ion patterns.[11] It is also worth noting that MS/MS product ion spectra and their associated mechanisms are strongly dependent on the collision energy conditions as proposed by Claeys and coworkers.[12]

Concerning the mechanisms associated with the formation of the various fragment ions, Saad and coworkers have proposed fragmentation pathways for both cross-ring and glycosidic cleavages in heparin-like disaccharides.[13] Concerning cross-ring cleavages, they have suggested stepwise mechanisms in which fragment ions are formed via a charge-remote

process (the negative sulfate group being not directly involved in the fragmentation pathway).[14, 15] Furthermore, Gross has shown that such charge-remote processes can occur under low-energy collisions regime.[16]

Quantum chemistry studies dealing with the collision induced dissociation of sugars are particularly scarce in the literature[17-19], and to our knowledge the fragmentation pathways of sulfated sugars have not been explored theoretically. The common way of studying fragmentation pathways by theoretical methods is based on the exploration of potential energy surface (PES). But quantum chemistry calculations on saccharides are particularly challenging and time-consuming, given the number of possible mechanisms and the very wide conformational space that has to be probed. Furthermore, a PES can give insights on statistical fragmentation but does not take into account any kinetic effect that can be important in determining the unimolecular reactivity of such molecules, as pointed out for other systems.[20-29] In the present work, we have adopted a different computational approach by performing MS/MS experiments "*in silico*" by means of QM+MM chemical dynamics simulations. The main idea is to simulate the CID impact, identify the fragments, and have direct access to dissociation mechanisms.

As shown in previous works for different chemical systems, chemical dynamic simulations can indeed be a useful tool in order to clarify the "short" time-scale behavior of chemical processes occurring during the CID events.[21, 23, 24, 26, 30-32] Recently, we also assessed the usefulness of chemical dynamics simulations for both reproducing experimental MS/MS spectra of a peptide-like molecule, and for proposing relevant dissociation mechanisms.[33] Fragmentation processes observed during our chemical dynamics simulations for the formation of the different fragment ions detected experimentally, turned to be in agreement with experiments and notably isotopic labeling.

In the present study, we explore for the first time the merits of using QM+MM direct dynamic simulations combined with MS/MS experiments on a small sugar system. Galactose-6-Sulfate (Figure 1) was chosen for its simplicity and its relative small size. In particular, we have addressed two different goals: (i) reproduce theoretically the experimental fragment ions observed, (ii) propose a detailed description of the fragmentation mechanisms of a prototypical negative sulfated monosaccharide.

2. MATERIALS AND METHODS

2.1 Mass spectrometry

Electrospray MS/MS mass spectra were recorded on a QSTAR PULSAR XL (Applied Biosystems/MDS Sciex) hybrid instrument (QqTOF) fitted with an "ionspray" source. Aqueous solutions of Galactose-6-sulfate (Gas-6S) (10^{-4} mol L^{-1}) were introduced into the source using direct infusion with a syringe pump at a flow rate of 4µl/min. Ionization of the sample was achieved by applying a voltage of -4.5 kV to the sprayer probe and by the use of a nebulizing gas (GAS1, air) surrounding the sprayer probe. The operating pressure of GAS1 was adjusted to 1.4 bars by means of an electronic board (pressure sensors) as a fraction of the air inlet pressure. The declustering potential DP (also referred to as "cone voltage" in other devices), defined as the difference in potential between the orifice plate and the skimmer (grounded), ranged from 20 to 120 V. The operating pressure of the curtain gas (N_2), which prevents air or solvent from entering the analyzer region, was adjusted to 0.7 bars by means of pressure sensors, as a fraction of the N_2 inlet pressure. To improve ion transmission and subsequent sensitivity during the experiments, the collision gas (CAD, N_2) was present at all times for collisional focusing in both the Q0 (ion guide preceding the quadrupole Q1 and located just after the skimmer) and Q2 (collision cell) sectors.

For MS/MS spectra, complexes of interest were mass selected using Q1, and allowed to collide with nitrogen as collision gas in the second quadrupole (Q2), the resulting fragment ions being analyzed by the time-of-flight (TOF) after orthogonal injection. Furthermore, MS/MS spectra were systematically recorded at various collision energies ranging from 7 eV to 36 eV in the laboratory frame (the collision energy is given by the difference between the potentials of Q0 and Q2). The CAD parameter, which controls the amount of N_2 introduced into Q2, was set to its minimum value in order to limit multiple ion–molecule collisions. Note that, as discussed in previous papers, MS/MS spectra are very likely obtained under ~~a~~ multiple-collision regime.[34, 35]

Gal-6S was purchased from Grampan-enzymes (Aberdeen, Scotland) and was used without further purification. All experiments were performed in 100% water purified with a Milli-Q water purification system.

2.2 Direct dynamic simulations

The potential energy function for the collision system, consisting of negative $[Gal\text{-}6S]^-$ (saccharide) and the collision gas (Ar) is described by :

$$V = V_{Saccharide^-} + V_{Ar-Saccharide} \qquad (1)$$

where $V_{saccharide^-}$ is the intramolecular potential of $[Gal\text{-}6S]^-$ and $V_{Ar\text{-}saccharide}$ is the $Ar[Gal\text{-}6S]^-$ intermolecular potential. The PM3 semi-empirical Hamiltonian has been used for the intramolecular potential. The reliability of semi-empirical Hamiltoninas to model CID processes was established in previous works.[33, 36]

The intermolecular potential is expressed as a sum of two-body terms between the collision gas and the atoms of $[Gal\text{-}6S]^-$ given by:

$$V_{Ar-Saccharide} = \sum_i A_{Ar-i} e^{-B_{Ar-i} r_{Ar-i}} + \frac{C_{Ar-i}}{r_{Ar-i}^9} \qquad (2)$$

where *i* runs over all the $[Gal\text{-}6S]^-$ atoms. This potential is purely repulsive – A, B and C are always positive. For CH, OH and CH_2 groups we used parameters developed by Meroueh and Hase [37] and they are listed in the supporting information (SI-A). Note that the same potential form of Eq. 2 was recently used to simulate CID of protonated urea[31], $[Ca(urea)]^{2+}$ [30] and protonated *N*-formylalanylamide [33], and in all three cases good agreements with experimental results were obtained. Nevertheless, in order to carry out the direct dynamic simulations of our system, it was necessary to first obtain the interaction potential between Ar and SO_3 moiety and between Ar and ROR'. A, B and C values of Eq. 2 for these groups were obtained by fitting *ab initio* interaction energy curves carried out at the QCISD(T)/6-31++G** level of theory. BSSE correction was also taken into account following the counterpoise method of Boys and Bernardi.[38, 39] Both potential energy curves as well as the values for A, B and C are given in results section 3.1.

Note that here, as previously mentioned, we used Ar in simulations while in experiments N_2 is used as collision gas. As we have recently shown in a simple model case,[31] the main difference is that Ar gas provides a more efficient energy transfer with respect to N_2 and higher reaction probability (55% vs 30% in the case of protonated urea [31]).

Chemical dynamics simulations were performed starting from the structure shown in Figure 1. In order to determine the initial geometry of Gal-6S, we have performed a systematic search of conformers using the semi-empirical PM3 Hamiltonian method with the molecular modeling computer program Spartan. [40] After this conformational analysis, the most stable geometries of these PM3-optimized structures were then re-optimized at DFT level. DFT geometries were obtained by using the B3LYP hybrid functional [41, 42] as implemented in the Gaussian03 series of programs.[43] They were first optimized with the 6-311+G* basis set. Relative energies were refined by using the larger 6-311++G** basis set. Harmonic vibrational spectra and zero-point vibrational energies (ZPVE) of optimized

structures were computed at the B3LYP/6-311+G* level. We have thus kept the most stable structure and used it as initial configuration for chemical dynamics simulations (Figure 1).

Initial conditions in position and momenta were chosen by adding a quasi-classical 300 K Boltzmann distribution of vibrational/rotational energies about the isomer's potential energy minima.[44-46] Energies for the normal modes of vibration were selected from a 300 K Boltzmann distribution. The resulting normal mode energies were partitioned between kinetic and potential energies by choosing a random phase for each normal mode. A 300 K rotational energy of RT/2 was added to each principal axis of rotation for the ion. Vibrational and rotational energies were transformed into Cartesian coordinates and momenta following well-known algorithms implemented in VENUS.[47, 48] The ion was then randomly rotated about its Euler angles to take into account the random directions of the Ar + $[Gal\text{-}6S]^-$ collisions. Relative velocities were then added to the Ar/$[Gal\text{-}6S]^-$ system consistently with the center-of-mass collision energy and impact parameter. Collision energy of 19.5 eV (450 kcal/mol) was considered, corresponding to laboratory frame energy of 22.5 eV (519 kcal/mol) that falls inside our experimental conditions. The impact parameter, $\boldsymbol{b}$, was randomly sampled between 0 and 2 Å. The trajectories were calculated using a software package consisting of the general chemical dynamics computer program VENUS 96 coupled to MOPAC.[49] MOPAC was used to calculate the potential energy and gradient for the protonated peptide intramolecular potential. The classical equations of motion were integrated using the velocity Verlet algorithm with a time step of 0.2 fs that gives energy conservation for both reactive and nonreactive trajectories, as for a system we recently investigated. [33] The trajectories were initiated at an ion-projectile distance of 15 Å, large enough to guarantee no interaction between the ion and the colliding atom, and halted at a distance of 300 Å to allow substantial intramolecular motion of the sugar ion. This corresponds to a total integration time of about 50 ps. A trajectory was also stopped if the ion dissociates. In that case, the criterion distance of 7 Å was also used to

guarantee no interactions between fragments. Approximately 6500 trajectories were performed.

3. RESULTS

3.1 Ar/Gal-6S intermolecular potential

As mentioned before, the general potential energy function is given in Eq.1 where $V_{Ar\text{-}saccharide}$ represents the Ar/saccharide analytical intermolecular potential. The intermolecular potential analytical function (shown in Eq. 2) depends on parameters for each atom type of the target molecule. In our system, the intermolecular potentials of Ar/C, Ar/O and Ar/H were described previously in the literature by Meroueh and Hase [37]. Intermolecular potential for interaction between Ar and atoms of ether and SO_3 groups was obtained in this work as described in the methods section. In order to calculate the intermolecular potential of an ether group (R-O-R'), we have chosen the simplest ether, dimethoxyether, CH_3-O-CH_3, and for CH_3 group we have used the A,B and C values reported by Meroueh and Hase[37]. The interaction potential between Ar and an O atom attached to two methyl groups was obtained by performing *ab initio* calculations for Ar interacting with CH_3-O-CH_3 along Ar - - O (C_2 symmetry) and Ar - - O (σ_h symmetry) axes. The resulting *ab initio* energy curves are plotted in Figure 2. The potential parameters derived from fitting the curves of the two body potential are listed in Table 1.

The two-body interaction potential between Ar and the atoms of a sulfate group was determined from two sets of scans for the Ar/SO_4^{2-} system. Intermolecular potentials were calculated along the Ar - - - O-S and Ar -- - S axes. The potential energy curves for these calculations are given in the Figure 3. As observed, *ab initio* and fitted curves are in very good agreement. The potential parameters A, B and C for the sulfate are also listed in Table 1.

3.2 Mass spectrometry and CID experiments

Due to the presence of the sulfate group, Gal-6S is studied in the negative-ion mode. Under the electrospray conditions used, the most abundant ion generated is $[Gal\text{-}6S]^-$, detected at *m/z* 259. This species was then mass-selected and allowed to collide with N_2. Figure 4a presents its MS/MS spectrum obtained at collision energy of 26 eV (laboratory frame). Several dissociation channels can be observed. However, only fragment ions with relative intensities higher than 2% will be considered in the following discussion. The peaks detected at *m/z* 199, *m/z* 169 and *m/z* 139 correspond to the loss of $C_nH_{2n}O_n$ blocks through cross-ring cleavages, with n=2,3 and 4, respectively. Moreover, these ions further dissociate by loss of SO_3 leading to *m/z* 119, *m/z* 89 and *m/z* 59, respectively.

Figure 4b shows the MS/MS spectra of *m/z* 199 ion which was generated by in-source fragmentation. Four dissociation channels were observed. The most prominent peak corresponding to the loss of $C_2H_4O_2$ is detected at *m/z* 139. The second one (*m/z* 119) corresponds to the loss of SO_3. Additional fragmentations at *m/z* 97, 81 and *m/z* 59 corresponding to the formation of $[HSO_4]^-$, HSO_3^- and $[C_2H_3O_2]^-$, respectively, are also detected. Scheme 1 summarizes the fragmentation products observed. The former ion systematically arises from the dissociation of both the precursor ion and cross ring fragments. The second appears to be the main dissociation product of *m/z* 139. An ion at m/z 80 is also detected. MS/MS experiments indicate that it comes from the sulfate ion (*m/z* 97), which expels an OH radical, therefore leading to the $SO_3^{\cdot-}$ radical ion. Finally, note that the loss of formaldehyde from *m/z* 199 leading to *m/z* 169 is not experimentally observed, indicating that the *m/z* 199 species arises directly from the precursor ion.

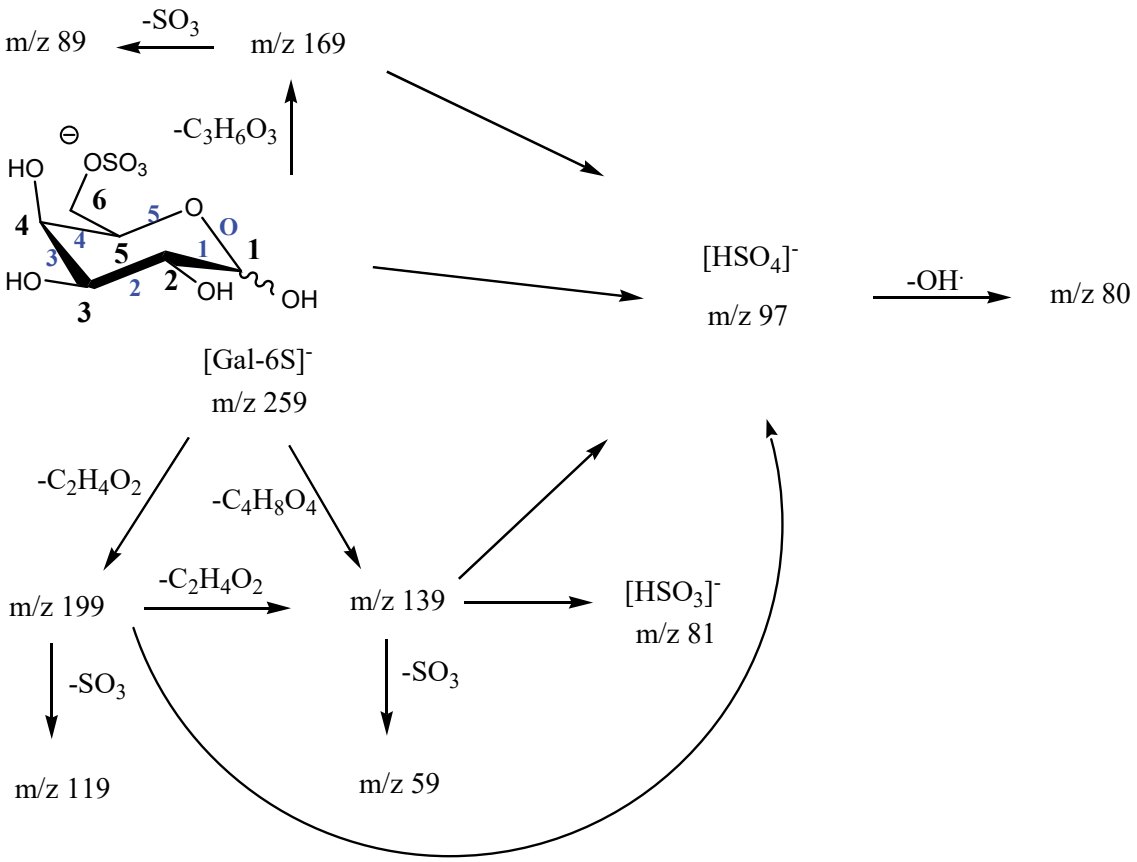

Scheme 1: Fragmentation scheme of Gal-6S upon collision as detected in MS/MS experiments

.

3.3 Chemical dynamic simulations

We have performed direct dynamic simulations of the $[Gal\text{-}6S]^-$ precursor ion, starting from the structure shown in Figure 1. Under the impact parameters and collision energy used, from approximately 6500 trajectories, a reactivity yield of 20% has been achieved. From chemical dynamics simulations we can obtain a so-called 'theoretical MS/MS spectrum' by counting the occurring of each fragment obtained after simulations of the collision. This spectrum is shown in Figure 5.

Table 2 lists the fragment ions observed experimentally (Figure 4a) and those that are present in the spectrum arising from chemical dynamic simulations. Remarkably, all the fragments observed experimentally but the *m/z* 119 (combined loss of $[C_2H_4O_2]$ and SO_3), are also present

in the theoretical MS/MS spectrum. One can also note that several fragment ions (*m/z* 213, 153, 131, 121, 109, 93, 75, 73 and 57) are obtained only theoretically, but most of them with a very small intensity in simulations. Other fragment ions correspond to ions of very low intensity in the experimental spectrum (*m/z* 149, 107, 81, 71). We should remark that chemical dynamics simulations are more aimed to explore the potential energy surface and, since we give relative high energy and simulations are on the ps time-length, we enhance fast processes, such that we can overestimate fragmentation pathways. Furthermore, some pathways can result as a limitation of the semi-empirical Hamiltonian. Thus, in the following, we use chemical dynamics mainly to explain fragmentation pathways of the experimentally observed fragments. We should note that from chemical dynamics simulations we obtained all the fragments observed experimentally but *m/z* 119. A possible way to account for the lack of such fragment in simulations is to make the assumption that it comes from the ion *m/z* 199 via a SO_3 loss. This is confirmed by the MS/MS spectrum of the *m/z* 199 ion, generated experimentally by in-source fragmentation of $[Gal\text{-}6S]^-$ (Figure 4b). Examination of Figure 4b indeed shows the presence of the *m/z* 119 ion thus confirming the loss of SO_3 from *m/z* 199. Consequently, two consecutive steps are necessary to generate the *m/z* 119. We can give at least two explanations about the absence of *m/z* 119 in chemical dynamics products : (i) the number of trajectories giving rise to *m/z* 199 ions was not very large and (ii) to let the system span into ion *m/z* 119, one should have carried out simulations with longer time-length.

In order to further confirm the origin of the *m/z* 119 fragment ions from *m/z* 199, several trajectories were carried out using the same conditions as described in section 2.2, starting from the structure 199_b (Supporting information figure SI-B1). Remarkably, they lead to the formation of the *m/z* 119 fragment ion (Supporting information 119.mpg). Consequently, the lack of *m/z* 119 fragment starting from Gal-6S may be explained by insufficient statistical

sampling in the simulations since the system probably needs more time to span the PES and open the *m/z* 119 reaction channel.

3.4 Fragments dissociation energies

In order to better discuss fragments obtained by chemical dynamics simulations, we have calculated the energies of different fragments at both PM3 and DFT level. Table 3 summarizes the dissociation energies for all the observed fragmentation pathways. We can first note that DFT and PM3 methods provide similar results. This is a partial assessment that PM3 reaction products are a good representation of DFT products. All the structures considered and their corresponding relative energies are reported in the supporting information SI-B. We will now use in the following discussion section energetics of the different dissociation routes, in order to better discuss the fragmentation pathways obtained from experiments and chemical dynamics simulations. After the collision with Ar, the ion is activated vibrationally and rotationally and the system has enough energy to evolve toward all the observed fragments. In supporting information SI-E, we show the vibrational and rotational energy of the activated Gal-6S$^-$ ion after the collision for non-reactive trajectories. We obtain an energy distribution that covers the energies required to obtain the product ions of Table 3. Thus, thermodynamically, the different ions are accessible almost equally (of course ions higher in energy need a larger energy transfer, but most of collisions seem to be able to activate up to those energies). The absence of *m/z* 119 in chemical dynamics done starting from the precursor ion, that has a similar energy than other fragments observed in simulations, is probably due, as mentioned before, to the fact that our simulation time-length is not sufficient because, probably, the pathway connecting the reactants to *m/z* 119 is kinetically more disfavored than others. We will detail reaction mechanisms in the next section.

4. Discussion

In this section, the fragmentation pathways observed by chemical dynamics are examined in detail, in order to determine the origin of each neutral loss observed in the experimental product ion spectra. Only fragment ions that are experimentally observed with relative intensities higher than 2% are considered in the discussion (the fragmentation pathways for the other fragments non-observed in experiments are given in Supporting information SI-D).

4.1 -[$C_2H_4O_2$] loss (*m/z* 199)

From the analysis of all the direct dynamic simulations, the loss of C_2-C_3 carbons is observed in all the trajectories associated with the elimination of [$C_2H_4O_2$], and occurs remote from the negative charge. As shown in Scheme 2, following the elimination of the neutral fragment, three structures (**A**, **B** and **C**) were found for *m/z* 199. The formation of the linear structure (**A**) was obtained in 12.5% of trajectories leading to *m/z* 199 (Supporting information 199_a.mpg). Furthermore, **A** can react giving two products: the acyclic structure (**B**) by a proton transfer from C_1 to C_4 as obtained in 50% of the cases (Supporting information 199_b.mpg), while for 37.5% of observed trajectories the structure we finally obtained was a 4-membered ring (C) (Supporting information 199_c.mpg).

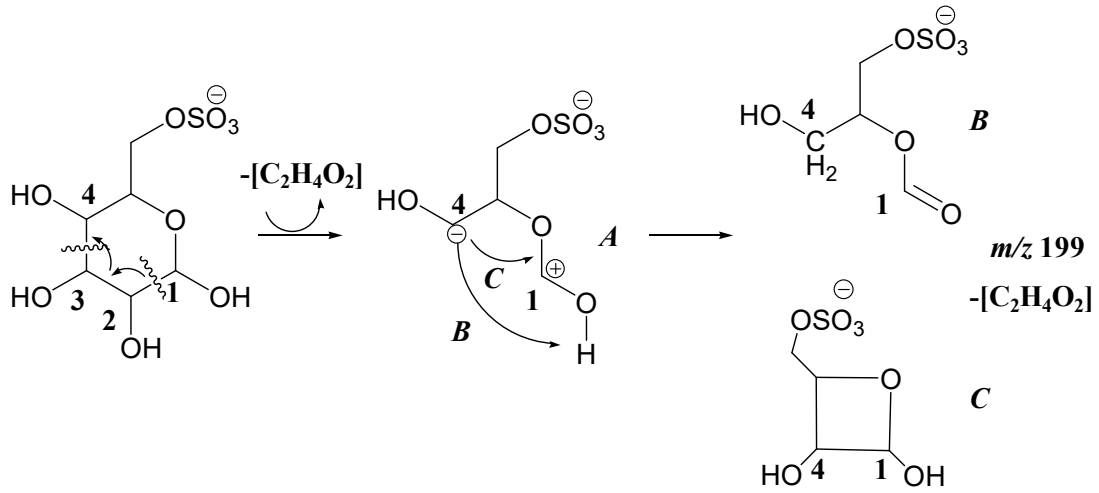

Scheme 2: Dissociation mechanism associated with the formation of *m/z* 199 (loss of [$C_2H_4O_2$]).

It is worth noting that this mechanism differs from those usually proposed in the literature by several aspects. First, the fragment ion presently generated formally corresponds to a $^{1,3}X$ ion, while the loss of $C_2H_4O_2$ from the reducing ring of saccharides is often associated with the formation of either $^{0,n}X$ or $^{0,n}A$ fragment ions.[50-55] In addition, the two bonds are presently simultaneously cleaved while it is usually assumed a stepwise process for the cross-ring cleavages, like in the fragmentation pathways proposed by Saad and coworkers for heparin disaccharides [13], and more generally for other types of saccharides.[50-55] According to some of these reports, loss of $C_2H_4O_2$ first requires the opening of the C-O endocyclic bond, followed by a proton transfer through a retro-aldol process.[13, 51, 54, 55] Note that in the present chemical dynamics simulations we model collisions at a relatively high energy (19.5 eV) and thus subsequent reactions are fast such that simultaneously bond cleavages are favored with respect to a stepwise process where the intermediate is not very stable.

4.2 -[$C_3H_6O_3$] loss (*m/z* 169)

From chemical dynamic simulations results (Scheme 3), the loss of $[C_3H_6O_3]$ is triggered by ring-opening between C_4 and C_5 (Supporting information 169.mpg). After this cleavage, a proton transfer occurs from the C_2 hydroxyl group to the carbon C_4. This proton transfer is followed by the second bond cleavage between C_1 and C_2 and the loss of $[C_3H_6O_3]$. This process therefore leads to the formation of a $^{2,4}X$ fragment ions. Once the neutral moiety eliminated, the newly-formed ion further rearranges through a second proton transfer from the carbon C_6 to the carbon C_1.

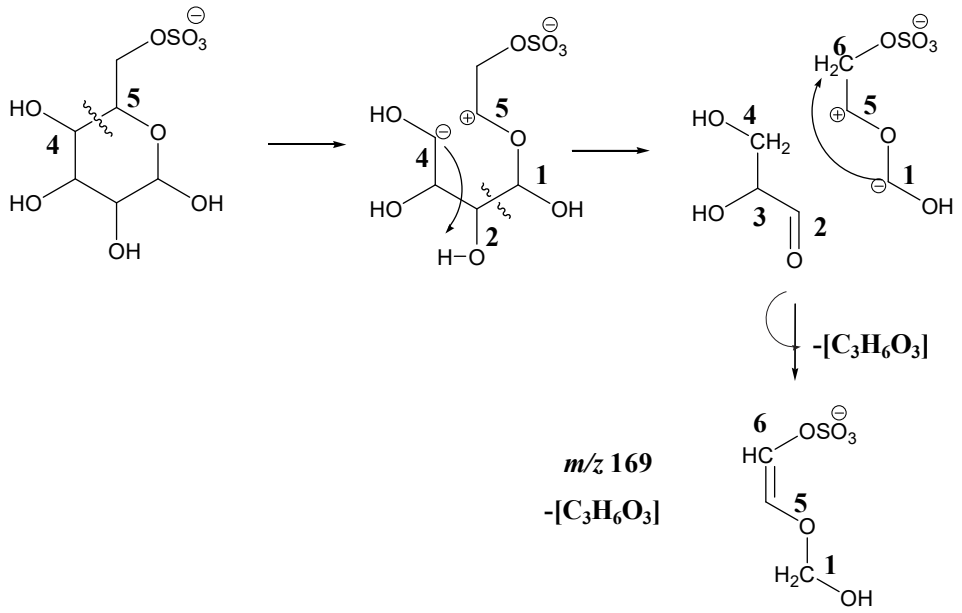

Scheme 3: Dissociation mechanism for formation of *m/z* 169 (loss of [C_3,H_6,O_3]).

The mechanisms associated with the elimination of $C_3H_6O_3$ have been scarcely studied. One may mention a study of Hofmeister *et al*., who proposed a totally different stepwise process initiated by the cleavage of the C-O endocyclic bond leading to a formyl group at C_1.[51] Then, the migration of this newly-formed carbonyl group onto position 2 followed by a McLafferty-like mechanism resulted in the elimination of $C_3H_6O_3$ and formation of a ^{0,3}A ion. This mechanism is therefore markedly different from the one observed during chemical dynamics simulations. Like for the loss of $C_2H_4O_2$, this finding suggests that in the case of sulfated saccharides, for which the negative charge is located onto the sulfate group, cross-ring cleavages may not be necessarily promoted by the cleavage of the C_1-O bond, which is known to be strongly activated for hexoses deprotonated onto the anomeric position.[19]

4.3 -[$C_4H_8O_4$] loss (*m/z* 139)

The loss of [$C_4H_8O_4$] leading to the *m/z* 139 fragment is the third type of cross-ring cleavage experienced by the precursor ion. As reported in Scheme 4, two different mechanisms may

account for this elimination (Supporting information 139_A.mpg and 139_B.mpg). For the first mechanism (**A**), fragments are obtained just after a single vibrational period (this corresponds to a fast process often called 'shattering mechanism' [31, 56, 57]). Three bonds are cleaved simultaneously (C_1-O_i, C_2-C_3 and C_4-C_5), and the loss of $C_4H_8O_4$ in fact corresponds to the elimination of two $C_2H_4O_2$ units, leading to a $^{0,4}A$ fragment ion. This mechanism is observed in 70% of the reactive trajectories providing *m/z* 139 as reaction products. Such concerted processes leading to two $C_2H_4O_2$ moieties, have already been proposed in order to account for experimental observations based upon labeling studies.[51, 54]

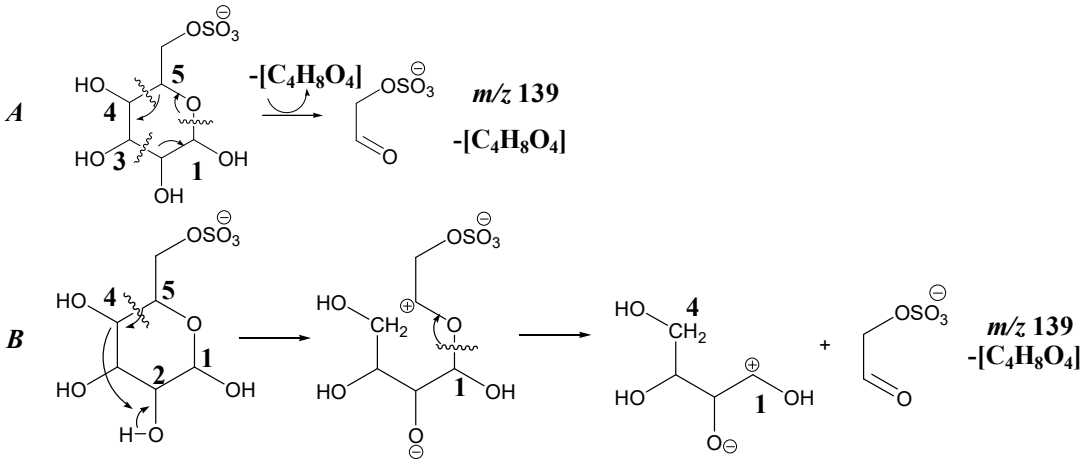

Scheme 4: Dissociation mechanism for formation of the *m/z* 139 ion (loss of $[C_4H_8O_4]$).

For the remaining 30% trajectories, the collision energy is first redistributed through the whole molecule and then the reaction proceeds. This mechanism starts with a proton transfer from the C_2 hydroxyl group to the carbon C_4, promoting the ring opening (C_4-C_5 bond cleavage). The C_1-O_i bond then breaks leading to the *m/z* 139 ion formation ($^{0,4}A$) and a $C_4H_8O_4$ neutral. Elimination of a single $C_4H_8O_4$ entity has been already suggested in the literature [51], but the mechanism proposed was markedly different, as it is implied in the first step the cleavage of C_1-O_i bond, generating a C1 formyl group. Then migration of the carbonyl group onto the C_3

position followed by a retro-aldol rearrangement promotes the scission of the C4-C5 bond. Remarkably, in both mechanisms the ion generated exhibits the same $[SO_3\text{-}O\text{-}CH_2\text{-}CHO]^-$ ion structure while the neutral fragment(s) eliminated is (are) different.

4.4 Formation of $[HSO_4]^-$ (*m/z* 97)

The discussion on the formation of the *m/z* 97 ion involves four different mechanisms (Supporting information 97_A.mpg, 97_B.mpg, 97_C.mpg and 97_D.mpg). Two of them, accounting for 85% of the reactive trajectories, are gathered in Scheme 5, the remaining mechanisms are given in the supporting information (SI-C). The first one (**A**) is observed in the 43% of the reactive trajectories. As shown in Scheme 5, the fragmentation starts with the cleavage of the C_6–O_S bond. Following this direct loss, a proton transfer from the carbon C_5 to the OSO_3^- group is observed.

The second mechanism (**B**) is observed for 42% of reactive trajectories. The fragmentation starts with the cleavage of the C_5–C_6 bond, followed by the consecutive losses of CH_2O and SO_3. Then, remarkably, the C_4 hydroxyl group moves to the SO_3, forming the HSO_4^-.

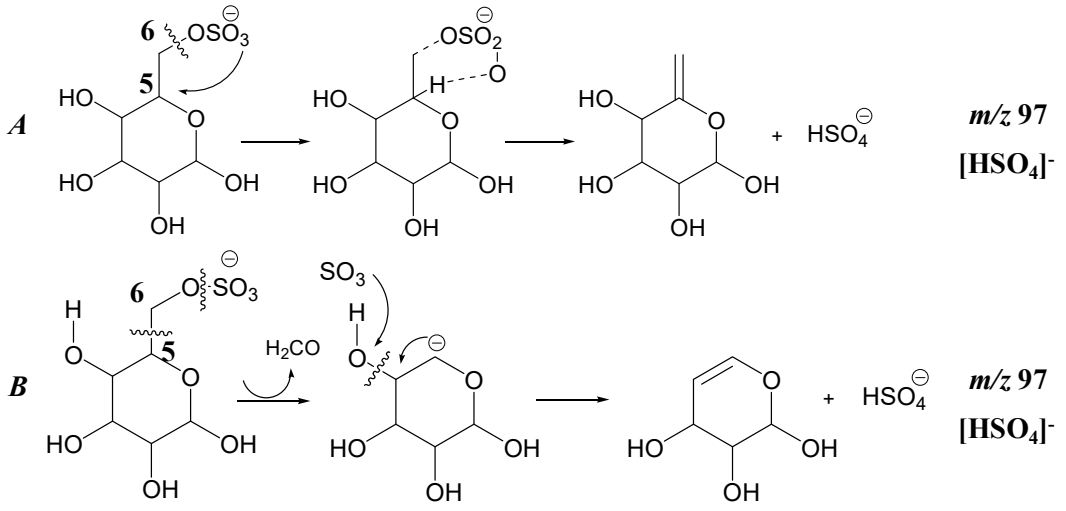

Scheme 5: Dissociation mechanism for formation of *m/z* 97 (formation of $[HSO_4]^-$)

4.5 -[$C_3H_6O_3$/SO_3] loss (*m/z* 89)

As shown in Scheme 6, generation of the *m/z* 89 ion starts by ring-opening between C_3 and C_4, remote from the negative group, followed by the rupture of the C_5–C_6 bond, and the consecutive neutral losses of CH_2O and SO_3 (promoted by the negative charge of the OSO_3^- group). Finally, elimination of C_2-C_3 carbons has been recorded after the C_1–C_2 bond cleavage. (Supporting information 89.mpg)

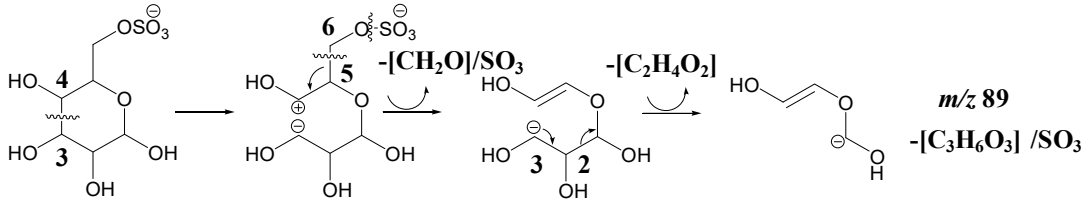

Scheme 6: Dissociation mechanism for formation of *m/z* 89 (elimination of $[C_3H_6O_3/SO_3]$).

4.6 -[$C_4H_8O_4$/SO_3]; formation of *m/z* 59

The *m/z* 59 fragment ion has been obtained by three different mechanisms summarized in Scheme 7 (Supporting information 59_A.mpg, 59_B.mpg and 59_C.mpg) Remarkably, the first step is common to all processes and implies cleavage of the C_5–C_6 bond and consecutive losses of CH_2O and SO_3, resulting in a negative charge formally located onto C_5. Then, mechanism (**A**), which amounts for 59% of the reactive trajectories, involves the ring opening by the scission of C_3-C_4 bond triggered by the negative charge, followed by the C_1–C_2 bond cleavage and the loss of $[C_3H_6O_3]$. Mechanism (**B**) (30% of the reactive trajectories) is associated with the subsequent cleavage of two bonds, namely C_4–C_5 and O_i–C_1, resulting in the formation of two neutral fragments. Finally, mechanism (**C**) was recorded for the remaining 11% of the reactive trajectories. This mechanism is rather similar to the (**A**) mechanism since it also involves the C_3-C_4 cleavage. In fact, the second bond cleavage (O_i–C_1) leads ultimately to the elimination of a $C_3H_6O_3$ moiety.

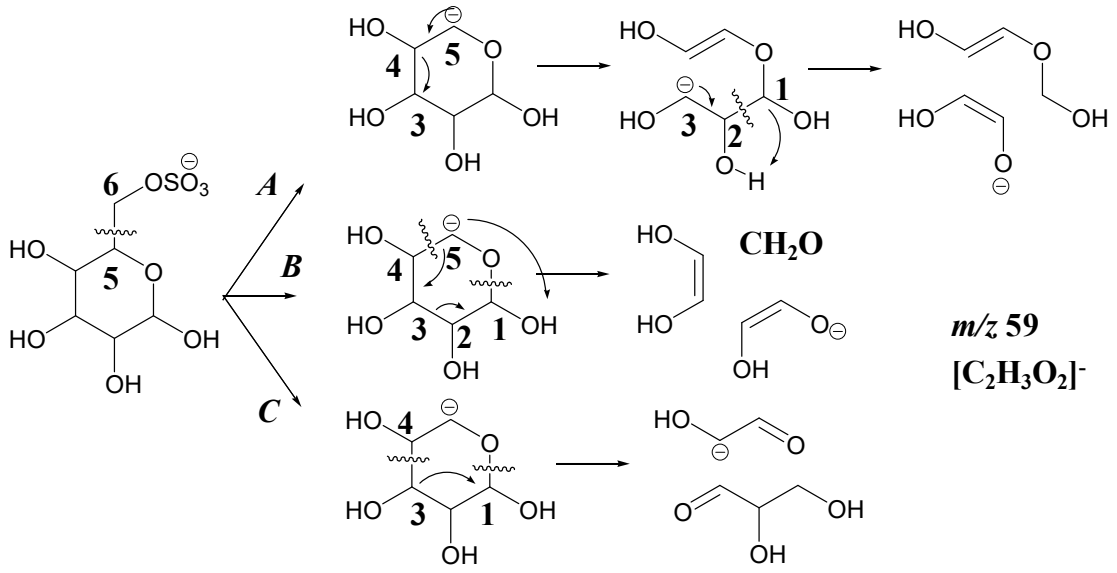

Scheme 7: Dissociation mechanism for formation of *m/z* 59 (loss of $[C_4H_8O_4/SO_3]$).

5.Conclusions

We show that chemical dynamics simulations can provide a good overview of the CID fragmentation process encountered for a sulfated monosaccharide. Remarkably, all the product ions but *m/z* 119, were successfully identified from the theoretical simulations. The lack of this fragment can be due to the short time-scale used in the simulation, which is not enough to let the system span first into *m/z* 199 and then into ion *m/z* 119, as also suggested by chemical dynamics simulations using *m/z* 199 as initial structure. The observed fragmentation pathways also suggest that although not observed experimentally, the species at *m/z* 149 arising from the consecutive losses of H_2CO and SO_3 could be transiently generated since it is involved in numerous mechanisms. Chemical dynamics also found, in agreement with previous experimental studies [14, 16], that the "charge-remote" model may be used in order to get a better understanding of the sugar behavior towards upon dissociation. In addition, our simulations reveal also that some reactions (i.e. formation of *m/z* 199) do not occur stepwise as previously suggested in the literature[13], under our energetic conditions from chemical dynamics simulations that show better shattering (i.e. non-statistical) mechanisms.

In agreement with our previous works, the use of a simple semiempirical Hamiltonian for the description of intramolecular ion interactions in the dynamics, needed to perform a correct statistical sampling for relative large systems, turned to be appropriate in supplying an explanation of the observed reactivity. Furthermore, in the present case, the reactions are able to proceed also through proton transfer (for which semiempirical methods can overestimate reaction barriers), maybe because the energy is sufficiently high to overcome these barriers. Concluding, the QM/MM direct dynamics simulations appeared to provide novel insights on the MS/MS fragmentation processes of sugars and allow rationalizing experimental findings.

Acknowledgments

This work was granted access to the HPC resources of CCRT under the allocations 2012082123 and 2013082123 made by GENCI (Grand Equipement National de Calcul Intensif). K.S. thanks UEVE for a visiting fellowship and partial support from the Basic Science Program through the National Research Foundation of Korea (KRF) administered by the Ministry of Education, Science and Technology (2012-0002654). Authors would also like to thank the LFB (Laboratoire français du Fractionnement et des Biotechnologies, Courtaboeuf, France) for the gift of the QSTAR PULSAR XL instrument.

FIGURE AND TABLE CAPTIONS

Figure 1: Chemical structure of Gal-6S.

Figure 2: *ab initio* (continuous line) and fitted (dotted line) for Ar/O(C2) in chart (a) and Ar/O(σh) in chart (b).

Figure 3: *ab initio* (continuous line) and fitted (pointed-line) for a) Ar - - - O-S and b) Ar -- - S axes.

Figure 4 MS/MS spectrum of **a**) $[Gal\text{-}6S]^-$ and of **b)** its m/z 199 fragment, both recorded at a collision energy of 26 eV (Laboratory frame).

Figure 5: Theoretical MS/MS spectrum for Gal-6S; in red color fragments that are observed on both theoretical and experimental MS/MS spectra.

Table 1: Parameters used in Eq. 2 with A, B and C in kcal/mol, $Å^{-1}$, $Å^9$ kcal/mol respectively

Table 2: Comparison between theoretical and experimental MS/MS spectra.

Table 3: Relative energies of different products at a) B3LYP/6-311+G* b) B3LYP/6-311++G** and c) PM3 levels of theory. Values are in kcal/mol

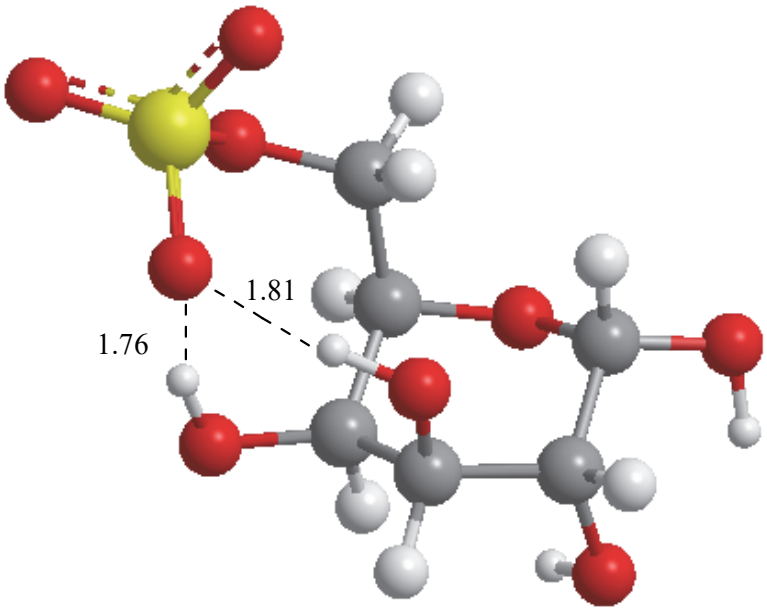

Figure 1

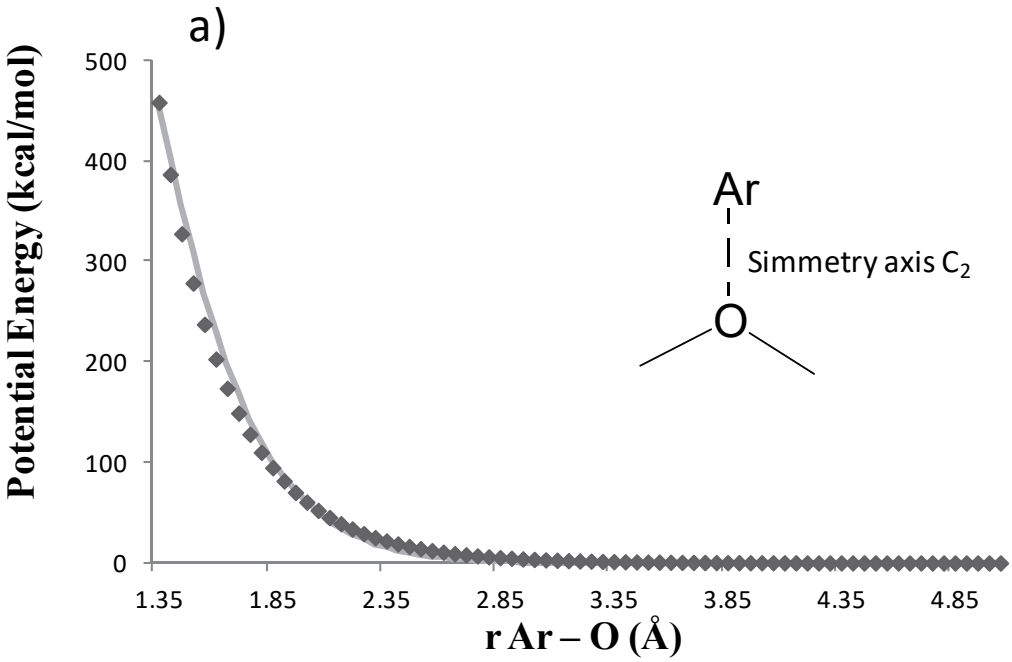
a)
Potential Energy (kcal/mol)
500
400
300
200
100
0
1.35
1.85
2.35
2.85
3.35
3.85
4.35
4.85
r Ar – O (Å)
Ar
Simmetry axis C2
O

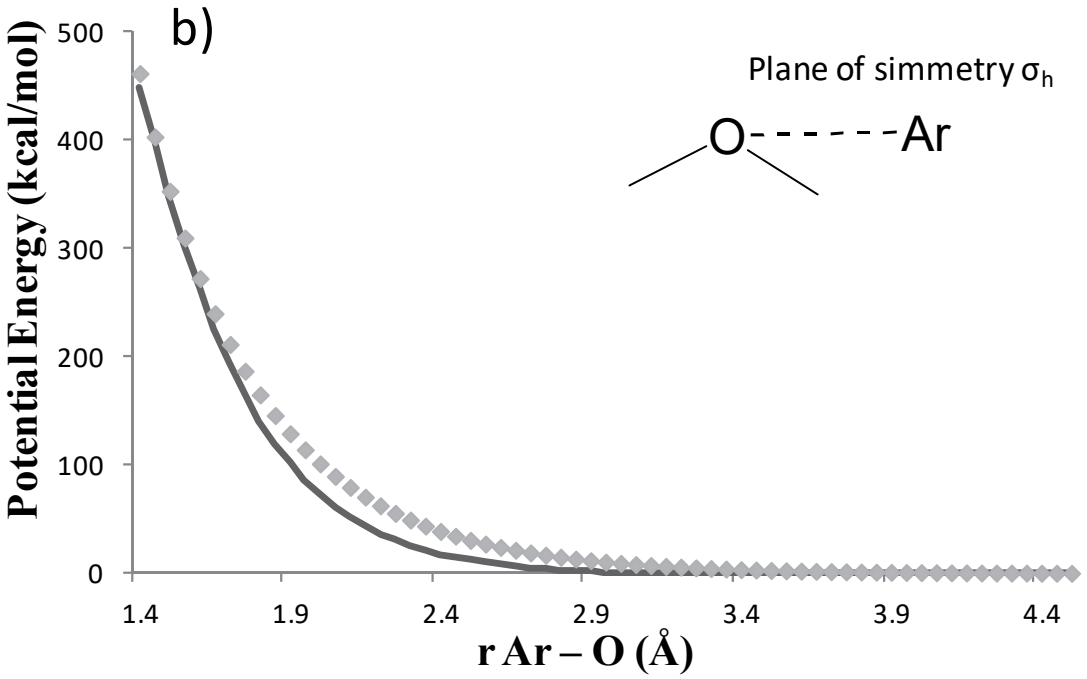
b)
Plane of simmetry σ_h
O------Ar
Potential Energy (kcal/mol)
500
400
300
200
100
0
1.4
1.9
2.4
2.9
3.4
3.9
4.4
r Ar – O (Å)

Figure 2

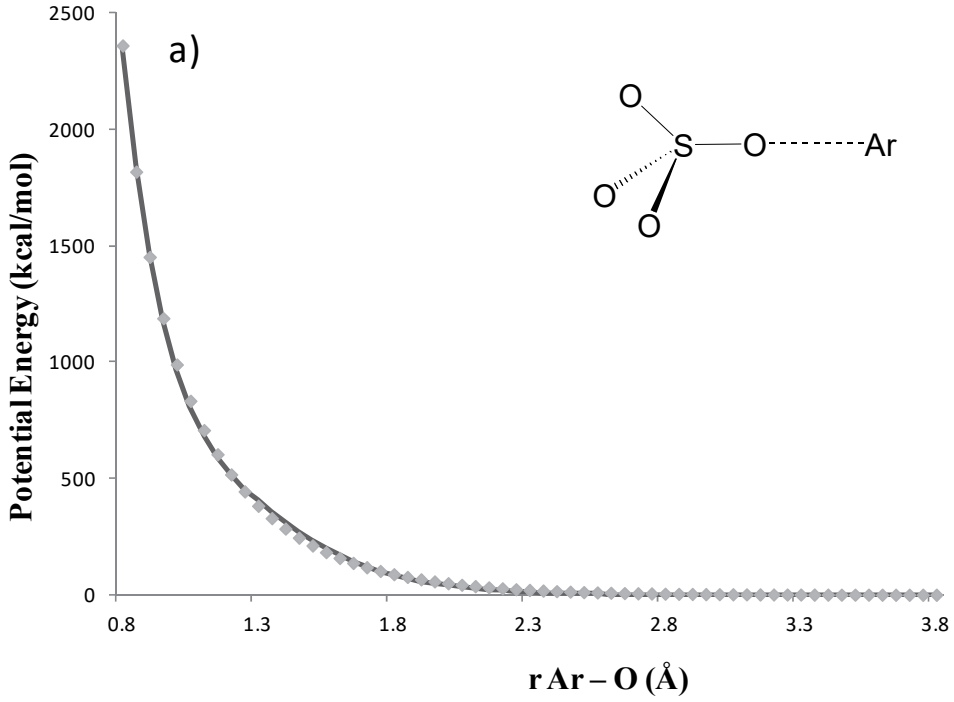
a)
O
S
O
Ar
O
O
Potential Energy (kcal/mol)
2500
2000
1500
1000
500
0
0.8
1.3
1.8
2.3
2.8
3.3
3.8
r Ar – O (Å)

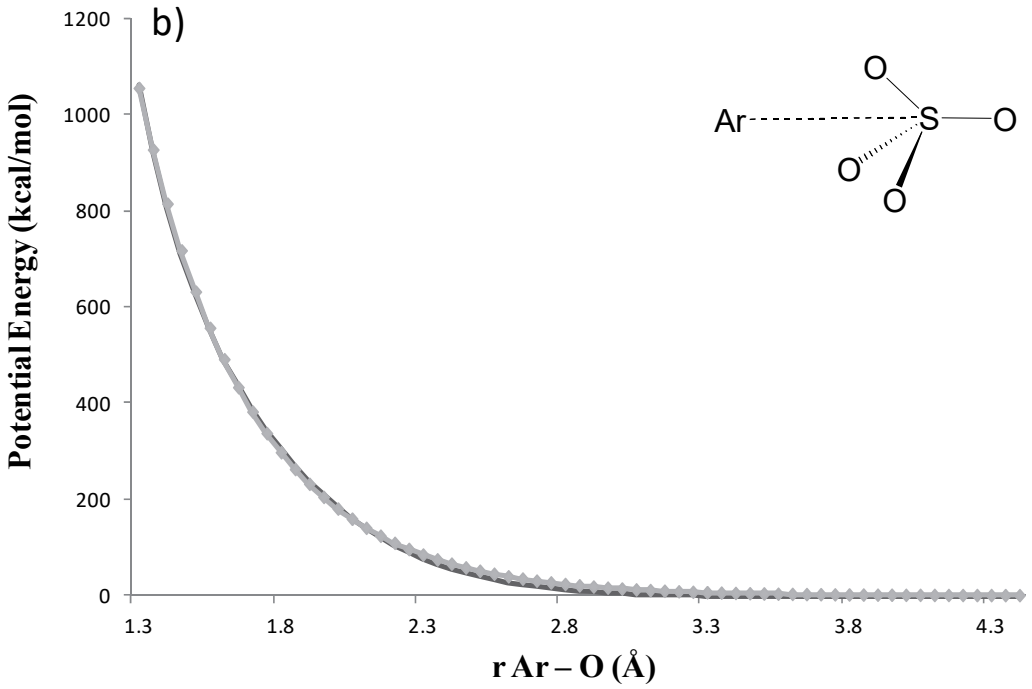
b)
Potential Energy (kcal/mol)
1200
1000
800
600
400
200
0
1.3
1.8
2.3
2.8
3.3
3.8
4.3
r Ar – O (Å)
Ar
S
O
O
O
O

Figure 3

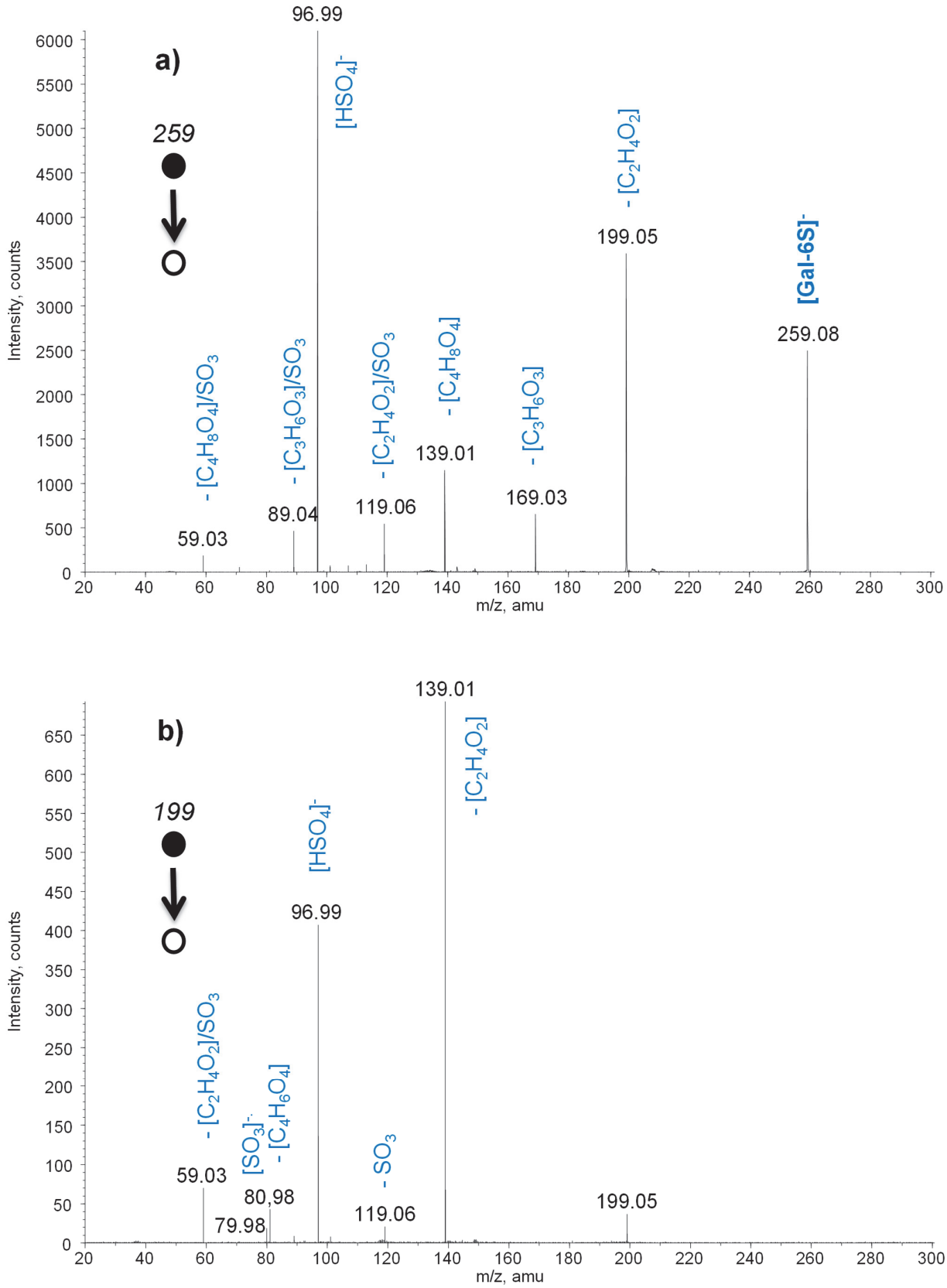
a)
259
96.99
[HSO4]-
- [C2H4O2]
199.05
[GaI-6S]-
259.08
- [C4H8O4]/SO3
- [C3H6O3]/SO3
- [C2H4O2]/SO3
- [C4H8O4]
- [C3H6O3]
139.01
169.03
89.04
119.06
59.03
Intensity, counts
m/z, amu
b)
199
139.01
- [C2H4O2]
[HSO4]-
96.99
- [C2H4O2]/SO3
[SO3]-
- [C4H6O4]
- SO3
59.03
80,98
79.98
119.06
199.05
Intensity, counts
m/z, amu

Figure 4

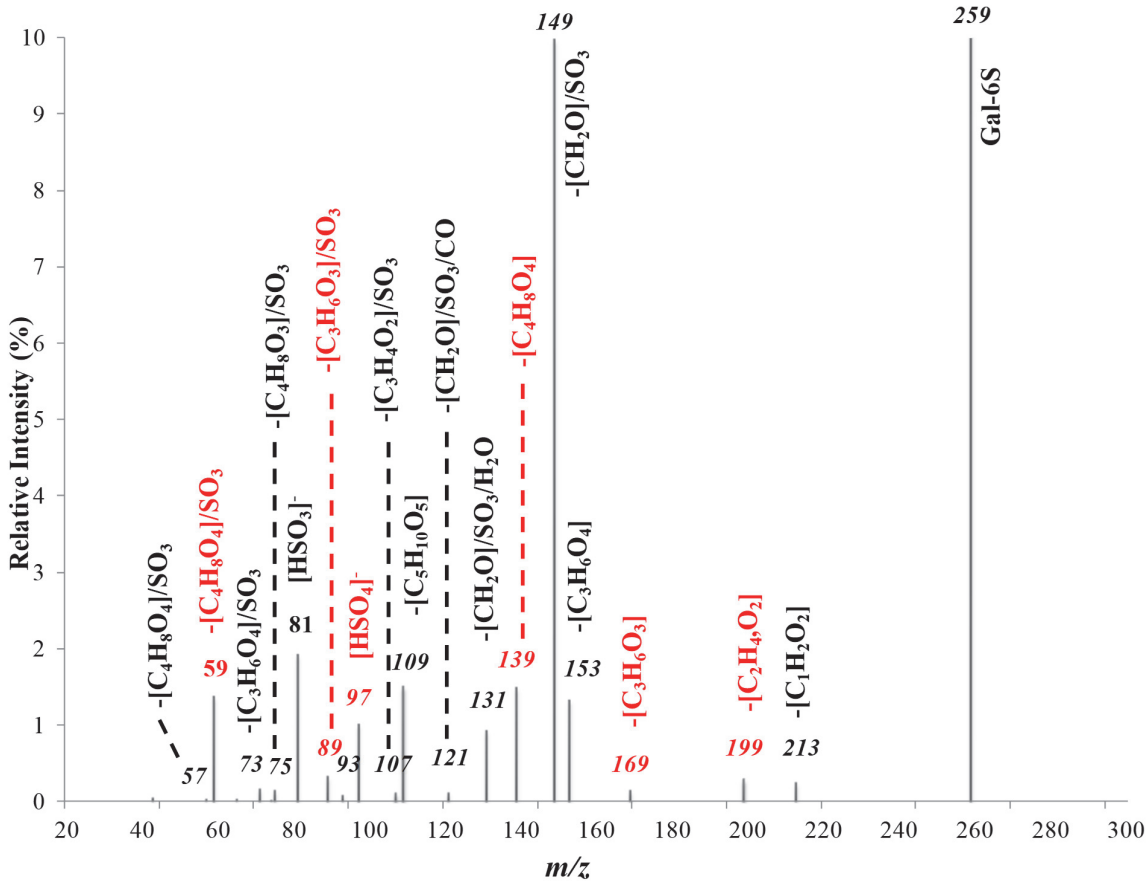
Relative Intensity (%)
m/z
Gal-6S
259
149
-[CH2O]/SO3
-[C4H8O4]/SO3
-[C3H6O4]/SO3
-[C4H8O3]/SO3
[HSO3]-
-[C3H6O3]/SO3
[HSO4]-
-[C3H4O2]/SO3
-[C5H10O5]
-[CH2O]/SO3/CO
-[CH2O]/SO3/H2O
-[C4H8O4]
-[C3H6O4]
-[C3H6O3]
-[C2H4,O2]
-[C1H2O2]
57
59
73
75
81
89
93
97
107
109
121
131
139
153
169
199
213

Figure 5

Potential	a	b	c
Ar/CH4(ArC)	11202.65	2.399515	152.7291
Ar/CH4(ArH)	8668.20	3.801426	1.727232
Ar/ROR'(ArO)	21672.61	3.201106	541.8338
Ar/O (SO_4)	15473.036	2.876424	105.7033
Ar/S (SO_4)	49444.7528	3.355363	90.95155

Table 1

m/z	Dissociation product	Exp.	QM/MM
213	-[$C_1H_2O_2$]		**X**
199	-[$C_2H_4O_2$]	**X**	**X**
169	-[$C_3H_6O_3$]	**X**	**X**
153	-[$C_3H_6O_4$]		**X**
149	-[CH_2O] /SO_3/CO	**X**[(a)]	**X**
139	-[$C_4H_8O_4$]	**X**	**X**
131	-[CH_2O]/SO_3/H_2O		**X**
121	-[CH_2O]/SO_3/CO		**X**
119	-[$C_2H_4O_2$] /SO_3	**X**	
109	-[$C_5H_{10}O_5$]		**X**
107	-[$C_3H_4O_2$]/SO_3	**X**[(a)]	**X**
97	[HSO_4]$^-$	**X**	**X**
93	-[$C_5H_{10}O_6$]		**X**
89	-[$C_3H_6O_3$]/SO_3	**X**	**X**
81	[HSO_3]$^-$	**X**[(a)]	**X**
75	-[$C_4H_8O_3$]/SO_3		**X**
73	-[$C_3H_6O_4$]/SO_3		**X**
71	-[$C_3H_6O_3$]/H_2O/SO_3	**X**[(a)]	**X**
59	-[$C_4H_8O_4$]/SO_3	**X**	**X**
57	-[$C_4H_8O_4$]/SO_3		**X**

(a) **:**trace amounts

Table 2

Product ion	ΔE^A	ΔE^B	ΔE^C
199_A	26.8	28.4	27.6
199_B	35.8	33.8	30.9
169	32.1	34.1	27.1
139_a	39.6	36.7	37.7
139_b	16.0	18.7	15.5
119_a	97.1	98.6	92.9
119_b	109.1	107.4	104.8
97_a	24.8	20.5	20.3
97_b	30.7	29.5	22.3
89	165.5	161.8	129.3
59_a	113.9	114.2	100.9
59_b	115.8	115.7	104.7
59_c	98.6	99.5	88.4

Table 3

REFERENCES

[1] R.A. Dwek, Glycobiology: Toward understanding the function of sugars, Chemical Reviews, 96 (1996) 683-720.
[2] J. Zaia, Mass spectrometry of oligosaccharides, Mass Spectrometry Reviews, 23 (2004) 161-227.
[3] Y.Q. Dai, R.M. Whittal, C.A. Bridges, Y. Isogai, O. Hindsgaul, L. Li, Matrix-assisted laser desorption ionization mass spectrometry for the analysis of monosulfated oligosaccharides, Carbohydrate Research, 304 (1997) 1-9.
[4] D.J. Harvey, Matrix-assisted laser desorption/ionization mass spectrometry of carbohydrates, Mass Spectrometry Reviews, 18 (1999) 349-450.
[5] C. Przybylski, F. Gonnet, Y. Hersant, D. Bonnaffe, H. Lortat-Jacob, R. Daniel, Desorption Electrospray Ionization Mass Spectrometry of Glycosaminoglycans and Their Protein Noncovalent Complex, Analytical Chemistry, 82 (2010) 9225-9233.
[6] K. Takagaki, K. Kojima, M. Majima, T. Nakamura, I. Kato, M. Endo, Ion-Spray Mass-Spectrometric Analysis Of Glycosaminoglycan Oligosaccharides, Glycoconjugate Journal, 9 (1992) 174-179.
[7] Y.S. Kim, M.Y. Alm, S.J. Wu, D.-H. Kim, T. Toida, L.M. Teesch, Y. Park, G. Yu, J. Lin, R.J. Linhardt, Determination of the structure of oligosaccharides prepared from acharan sulfate, Glycobiology, 8 (1998) 869-877.
[8] J. Zaia, J.E. McClellan, C.E. Costello, Tandem mass spectrometric determination of the 4S/6S sulfation sequence in chondroitin sulfate oligosaccharides, Analytical Chemistry, 73 (2001) 6030-6039.
[9] J.E. McClellan, C.E. Costello, P.B. O'Connor, J. Zaia, Influence of charge state on product ion mass spectra and the determination of 4S/6S sulfation sequence of chondroitin sulfate oligosaccharides, Analytical Chemistry, 74 (2002) 3760-3771.
[10] J. Zaia, C.E. Costello, Tandem mass Spectrometry of sulfated heparin-like glycosaminoglycan oligosaccharides, Analytical Chemistry, 75 (2003) 2445-2455.
[11] E.F. Naggar, C.E. Costello, J. Zaia, Competing fragmentation processes in tandem mass spectra of heparin-like Glycosaminoglycans, Journal of The American Society for Mass Spectrometry, 15 (2004) 1534-1544.
[12] M. Claeys, H. VandenHeuvel, S. Chen, P.J. Derrick, F.A. Mellon, K.R. Price, Comparison of high- and low-energy collision-induced. Dissociation tandem mass spectrometry in the analysis of glycoalkaloids and their aglycons, Journal of The American Society for Mass Spectrometry, 7 (1996) 173-181.
[13] O.M. Saad, J.A. Leary, Delineating mechanisms of dissociation for isomeric heparin disaccharides using isotope labeling and ion trap tandem mass spectrometry, Journal of The American Society for Mass Spectrometry, 15 (2004) 1274-1286.
[14] J. Adams, Charge-Remote Fragmentations - Analytical Applications And Fundamental-Studies, Mass Spectrometry Reviews, 9 (1990) 141-186.
[15] M.L. Gross, Charge-Remote Fragmentations - Method, Mechanism And Applications, International Journal of Mass Spectrometry and Ion Processes, 118 (1992) 137-165.
[16] M.L. Gross, Charge-remote fragmentation: an account of research on mechanisms and applications, International Journal of Mass Spectrometry, 200 (2000) 611-624.
[17] J.A. Carroll, D. Willard, C.B. Lebrilla, Energetics of Cross-Ring Cleavages and Their Relevance to the Linkage Determination of Oligosaccharides, Analytica Chimica Acta, 307 (1995) 431-447.
[18] M. Alcami, A. Luna, O. Mo, M. Yanez, L. Boutreau, J. Tortajada, Experimental and theoretical investigation of the reactions between glucose and Cu+ in the gas phase, Journal of Physical Chemistry A, 106 (2002) 2641-2651.

[19] J.Y. Salpin, J. Tortajada, Gas-phase acidity of D-glucose. A density functional theory study, Journal of Mass Spectrometry, 39 (2004) 930-941.
[20] P.T. Fenn, Y.J. Chen, S. Stimson, C.Y. Ng, Dissociation of CH3SH+ by Collisional Activation: Evidence of Nonstatistical Behavior†, Journal of Physical Chemistry A, 101 (1997) 6513-6522.
[21] E. Martinez-Nunez, S.A. Vazquez, J.M.C. Marques, Quasiclassical trajectory study of the collision-induced dissociation of CH3SH++Ar, Journal of Chemical Physics, 121 (2004) 2571-2577.
[22] Y.J. Chen, P.T. Fenn, K.-C. Lau, C.Y. Ng, C.-K. Law, W.-K. Li, Study of the Dissociation of CH3SCH3+ by Collisional Activation: Evidence of Nonstatistical Behavior†, Journal of Physical Chemistry A, 106 (2002) 9729-9736.
[23] E. Martinez-Nunez, S.A. Vazquez, F.J. Aoiz, J.F. Castillo, Quasiclassical trajectory study of the collision-induced dissociation dynamics of Ar+CH3SH+ using an ab initio interpolated potential energy surface, Journal of Physical Chemistry A, 110 (2006) 1225-1231.
[24] E. Martinez-Nunez, A. Fernandez-Ramos, S.A. Vazquez, J.M.C. Marques, M.Y. Xue, W.L. Hase, Quasiclassical dynamics simulation of the collision-induced dissociation of Cr(CO)(6)(+) with Xe, Journal of Chemical Physics, 123 (2005) 154311.
[25] J.B. Liu, K. Song, W.L. Hase, S.L. Anderson, Direct dynamics study of energy transfer and collision-induced dissociation: Effects of impact energy, geometry, and reactant vibrational mode in H2CO+-Ne collisions, Journal of Chemical Physics, 119 (2003) 3040-3050.
[26] S.O. Meroueh, Y.F. Wang, W.L. Hase, Direct dynamics Simulations of collision- and surface-induced dissociation of N-protonated glycine. Shattering fragmentation, Journal of Physical Chemistry A, 106 (2002) 9983-9992.
[27] U. Lourderaj, W.L. Hase, Theoretical and Computational Studies of Non-RRKM Unimolecular Dynamics†, Journal of Physical Chemistry A, 113 (2009) 2236-2253.
[28] T. Beyer, Swinehar.Df, NUMBER OF MULTIPLY-RESTRICTED PARTITIONS, Commun. ACM, 16 (1973) 379-379.
[29] G. Vayner, S.V. Addepalli, K. Song, W.L. Hase, Post-transition state dynamics for propene ozonolysis: Intramolecular and unimolecular dynamics of molozonide, Journal of Chemical Physics, 125 (2006).
[30] R. Spezia, A. Cimas, M.-P. Gaigeot, J.-Y. Salpin, K. Song, W.L. Hase, Collision Induced Dissociation of Doubly-charged Ions : Coulomb Explosion vs Neutral Loss in [Ca(urea)]2+ Gas Phase Unimolecular Reactivity via Chemical Dynamics Simulations, Physical Chemistry Chemical Physics, 14 (2012) 11724-11736.
[31] R. Spezia, J.-Y. Salpin, M.-P. Gaigeot, W.L. Hase, K. Song, Protonated Urea Collision-Induced Dissociation. Comparison of Experiments and Chemical Dynamics Simulations, Journal of Physical Chemistry A, 113 (2009) 13853-13862.
[32] Y. Jeanvoine, M.P. Gaigeot, W.L. Hase, K. Song, R. Spezia, Collision induced dissociation of protonated urea with N-2: Effects of rotational energy on reactivity and energy transfer via chemical dynamics simulations, International Journal of Mass Spectrometry, 308 (2011) 289-298.
[33] D. Ortiz, P. Martin-Gago, A. Riera, K. Song, J.-Y. Salpin, R. Spezia, Gas-phase collision induced dissociation mechanisms of peptides: Theoretical and experimental study of N-formylalanylamide fragmentation, International Journal of Mass Spectrometry, 335 (2013) 33-44.
[34] C. Trujillo, O. Mó, M. Yáñez, J. Tortajada, J.Y. Salpin, Selenourea-Ca^{2+} reactions in gas phase. Similarities and dissimilarities with urea and thiourea, Journal of Physical Chemistry B, 112 (2008) 5479-5486.

[35] A. Eizaguirre, O. Mo, M. Yanez, J.Y. Salpin, Modeling the interactions between peptide functions and Sr(2+): formamide-Sr(2+) reactions in the gas phase, Physical Chemistry Chemical Physics, 13 (2011) 18409-18417.
[36] K.S. H.Bednarski, M.Domański, J.Weszka, G.Adamus, M.Kowalczuk, V.Cozan,, A combined theoretical and experimental study of mechanisms of fragmentation active for PHB oligomers in negative-ion mode multistage mass spectrometry, Int. J. Mass Spectrom, 304 (2011) 15-24.
[37] O. Meroueh, W.L. Hase, Collisional activation of small peptides, Journal of Physical Chemistry A, 103 (1999) 3981-3990.
[38] S.F. Boys, F. Bernardi, Calculation Of Small Molecular Interactions By Differences Of Separate Total Energies - Some Procedures With Reduced Errors, Molecular Physics, 19 (1970) 553-&.
[39] S. Simon, M. Duran, J.J. Dannenberg, How does basis set superposition error change the potential surfaces for hydrogen bonded dimers?, Journal of Chemical Physics, 105 (1996) 11024-11031.
[40] M. Kawatsura, J.F. Hartwig, Simple, highly active palladium catalysts for ketone and malonate arylation: Dissecting the importance of chelation and steric hindrance, Journal of the American Chemical Society, 121 (1999) 1473-1478.
[41] A.D. Becke, Density-functional Thermochemistry .3. the Role of Exact Exchange., Journal of Chemical Physics, 98 (1993) 5648-5652.
[42] C. Lee, W. Yang, R.G. Parr, Development of the Colle-Salvetti correlation-energy formula into a functional of the electron density, Physical Reviews B, 37 (1988) 785-789.
[43] M.J. Frisch, G.W. Trucks, H.B. Schlegel, G.E. Scuseria, M.A. Robb, J.R. Cheeseman, V.G. Zakrzewski, J. J. A. Montgomery, T. Vreven, K.N. Kudin, J.C. Burant, J.M. Millam, S.S. Iyengar, J. Tomasi, V. Barone, B. Mennucci, M. Cossi, G. Scalmi, N. Rega, G.A. Petersson, H. Nakatsuji, M. Hada, M. Ehara, K. Toyota, R. Fukuda, J. Hasegawa, M. Ishida, T. Nakajima, Y. Honda, O. Kitao, C. Adamo, J. Jaramillo, R. Gomperts, R.E. Stratmann, O. Yazyev, J. Austin, R. Cammi, C. Pomelli, J. Ochterski, P.Y. Ayala, K. Morokuma, G.A. Voth, P. Salvador, J.J. Dannenberg, V.G. Zakrzewski, S. Dapprich, A.D. Daniels, M.C. Strain, O. Farkas, D.K. Malick, A.D. Rabuck, K. Raghavachari, J.B. Foresman, J.V. Ortiz, Q. Cui, A.G. Baboul, S. Clifford, J. Cioslowski, B.B. Stefanov, G. Liu, A. Liashenko, P. Piskorz, I. Komaromi, R.L. Martin, D.J. Fox, T. Keith, M.A. Al-Laham, C.Y. Peng, A. Nanayakkara, M. Challacombe, P.M.W. Gill, B. Johnson, W. Chen, M.W. Wong, C. Gonzalez, J.A. Pople, Gaussian03, in, Gaussian, Inc., Wallingford CT, 2003.
[44] S. Chapman, D.L. Bunker, Exploratory Study Of Reactant Vibrational Effects In Ch3 + H2 And Its Isotopic Variants, Journal of Chemical Physics, 62 (1975) 2890-2899.
[45] W.L. Hase, Y.J. Cho, Trajectory Studies Of S-N2 Nucleophilic-Substitution .3. Dynamic Stereochemistry And Energy-Transfer Pathways For The Cl-+Ch3cl Association And Direct Substitution-Reactions, Journal of Chemical Physics, 98 (1993) 8626-8639.
[46] C.S. Sloane, W.L. Hase, Dynamics Of State Selected Unimolecular Reactions - Chloroacetylene Dissociation And Predissociation, Journal of Chemical Physics, 66 (1977) 1523-1533.
[47] X.C. Hu, W.L. Hase, T. Pirraglia, Vectorization of the General Monte Carlo Classical Trajectory Program VENUS, Journal of Computational Chemistry, 12 (1991) 1014-1024.
[48] W.L. Hase, Duchovic, R,J.; Hu, X.; Komornicki, A.; Lim, K.;Lu, D-H.; Peslherbe, G.H.; Swamy, K.N.; Vande Linde, S.R.; Wang, H.;Wolf, R.J., VENUS96, a General Chemical Dynamics Computer Program, QCPE, 16 (1996).
[49] J.J.P. Stewart, Special Issue -MOPAC- A semiempirical molecular-orbital program, J. Comput.-Aided Mol. Des., 4 (1990) 1-45.

[50] Z.R. Zhou, S. Ogden, J.A. Leary, Linkage Position Determination in Oligosaccharides - Ms/Ms Study of Lithium-Cationized Carbohydrates, Journal of Organic Chemistry, 55 (1990) 5444-5446.
[51] G.E. Hofmeister, Z. Zhou, J.A. Leary, Linkage Position Determination in Lithium-Cationized Disaccharides - Tandem Mass-Spectrometry and Semiempirical Calculations, Journal of the American Chemical Society, 113 (1991) 5964-5970.
[52] S.P. Gaucher, J.A. Leary, Stereochemical differentiation of mannose, glucose, galactose, and talose using zinc(II) diethylenetriamine and ESI-ion trap mass spectrometry (vol 70, pg 3009, 1998), Analytical Chemistry, 70 (1998) 3337-3337.
[53] G. Smith, J.A. Leary, Mechanistic studies of diastereomeric nickel(II) N-glycoside complexes using tandem mass spectrometry, Journal of the American Chemical Society, 120 (1998) 13046-13056.
[54] J.Y. Salpin, J. Tortajada, Gas-phase reactivity of lead(II) ions with D-glucose. Combined electrospray ionization mass spectrometry and theoretical study, Journal of Physical Chemistry A, 107 (2003) 2943-2953.
[55] W. Tuting, R. Adden, P. Mischnick, Fragmentation pattern of regioselectively O-methylated maltooligosaccharides in electrospray ionisation-mass spectrometry/collision induced dissociation, International Journal of Mass Spectrometry, 232 (2004) 107-115.
[56] D.G. Schultz, L. Hanley, Shattering of SiMe3+ during surface-induced dissociation, Journal of Chemical Physics, 109 (1998) 10976-10983.
[57] T. Raz, R.D. Levine, On the shattering of clusters by surface impact heating, Journal of Chemical Physics, 105 (1996) 8097-8102.

Galactose 6-sulfate collision induced dissociation from QM+MM chemical dynamics simulations and ESI-MS/MS experiments.

*Daniel Ortiz,[1,2] Jean-Yves Salpin[*1,2] Kihyung Song[3] and Riccardo Spezia[*1,2]*

1) Université d'Evry Val d'Essonne - Laboratoire Analyse et Modélisation pour la biologie et l'Environnement, Boulevard François Mitterrand, 91025 Evry Cedex (France).
2) CNRS- UMR 8587.
3) Department of Chemistry, Korea National University of Education, Chungbuk, Republic of Korea
Correspondence to:riccardo.spezia@univ-evry.fr; jean-yves.salpin@univ-evry.fr

Supporting Information

Table of Contents:

SI-A: CH, OH and CH_2 Intermolecular potential parameters

Table SI-A: Parameters for eqn(2) from Meroueh work [1] with a,b and c in kcal/mol, Å-1, and kcal Å/mol respectively.

$$V_{Ar-Saccharide} = \sum_i A_{Ar-i} e^{-B_{Ar-i} r_{Ar-i}} + \frac{C_{Ar-i}}{r_{Ar-i}^9} \qquad (2)$$

Potential	a	b	c
Ar/CH_4(ArC)	11202.65	2.399515	152.7291
Ar/CH_4(ArH)	8668.20	3.801426	1.727232
Ar/HCO_2H(ArCO)	8471.33	4.648228	304.6066
Ar/HCO_2H(ArOC)	12914.72	2.681826	99.56698

[1] Meroueh O, Hase WL. Collisional activation of small peptides. *J. Phys. Chem. A* 1999; 103: 3981-3990.

SI-B: Structure and relative energies

Product ion	E1[A]	ZPE[A]	E2[B]	E1[C]	ZPE[C]
Gal-6S	-1310.76524	0.201863	-1310.799673	-0.726211	0.195495
199_A	-1081.62097	0.130480	-1081.635348	-0.551014	0.122578
199_B	-1081.60861	0.132296	-1081.62852	-0.551034	0.127743
169	-967.036020	0.096432	-967.048729	-0.466564	0.091348
139	-852.503140	0.063279	-852.507148	-0.413216	0.059154
119_a	-457.646347	0.112214	-457.660842	-0.277815	0.110302
119_b	-457.630270	0.115137	-457.649737	-0.261792	0.113246
97	-699.830066	0.026202	-699.836716	-0.365647	0.022658
89	-342.989736	0.076436	-343.009446	-0.160229	0.078717
59	-228.527043	0.047316	-228.538241	-0.140406	0.048073

Table SI_B1: Total (Hartree) energies of product ions.

Neutral loss	E1[A]	ZPE[A]	E2[B]	E1[C]	ZPE[C]
[CH_2O]	-114.538944	0.026580	-114.541847	-0.054363	0.026124
[$C_2H_4O_2$]	-229.091098	0.060793	-229.108661	-0.119071	0.060644
[$C_3H_4O_2$]	-267.213289	0.066613	-267.224936	-0.104386	0.065704
[$C_3H_6O_3$]	-343.666884	0.094092	-343.685434	-0.205289	0.092794
[$C_3H_6O_3$]_c	-343.663818	0.093936	-343.682800	-0.185134	0.092429
[$C_4H_8O_4$]	-458.224966	0.126854	-458.251172	-0.277373	0.125353
[$C_5H_8O_4$]	-496.333961	0.135605	-496.360849	-0.257822	0.133763
[$C_5H_{10}O_5$]	-572.795450	0.164528	-572.828906	-0.357256	0.160584
[$C_6H_{10}O_5$]	-610.888495	0.168354	-610.923176	-0.321932	0.166477
[$C_6H_{10}O_6$]	-686.143042	0.173288	-686.176637	-0.405534	0.171453
CO	-113.349050	0.005041	-113.349050	-0.031493	0.005253
SO_3	-623.856479	0.011633	-623.856479	-0.166785	0.009421
H_2O	-76.443809	0.021215	-76.458431	-0.085020	0.021870

Table SI_B2: Total (Hartree) energies of the neutral losses

A=B3LYP/6-311+G*

B=B3LYP/6-311++G**

C=PM3

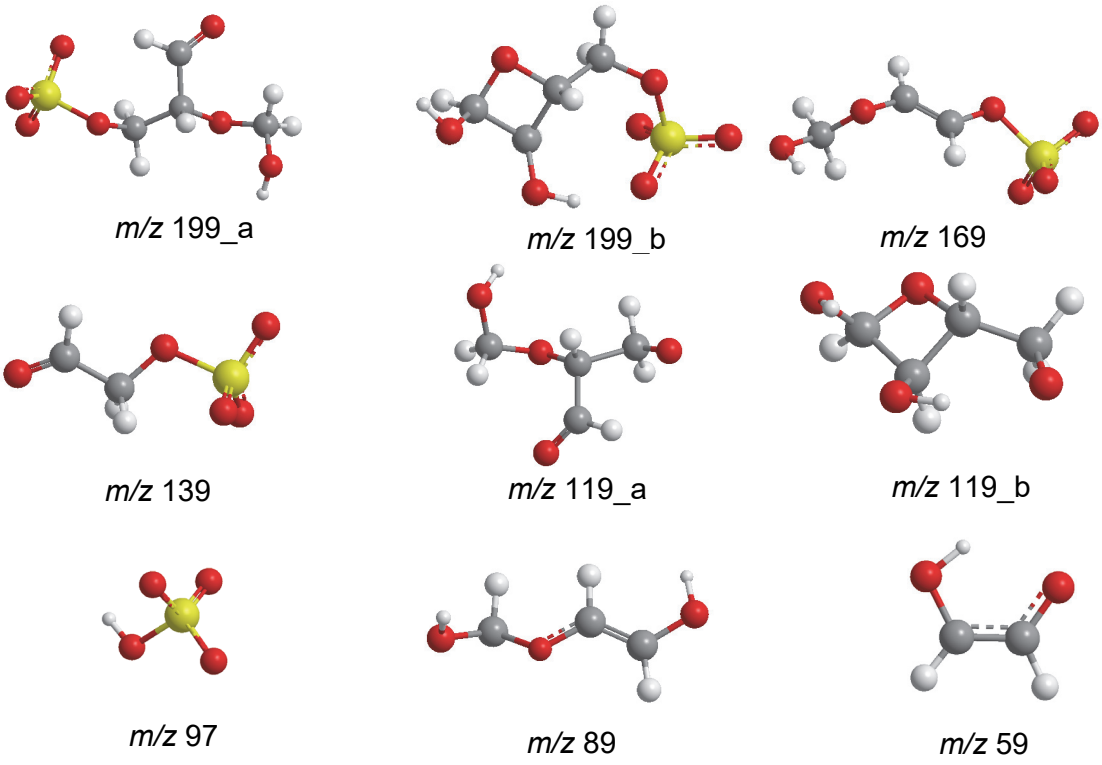

Figure SI-B1

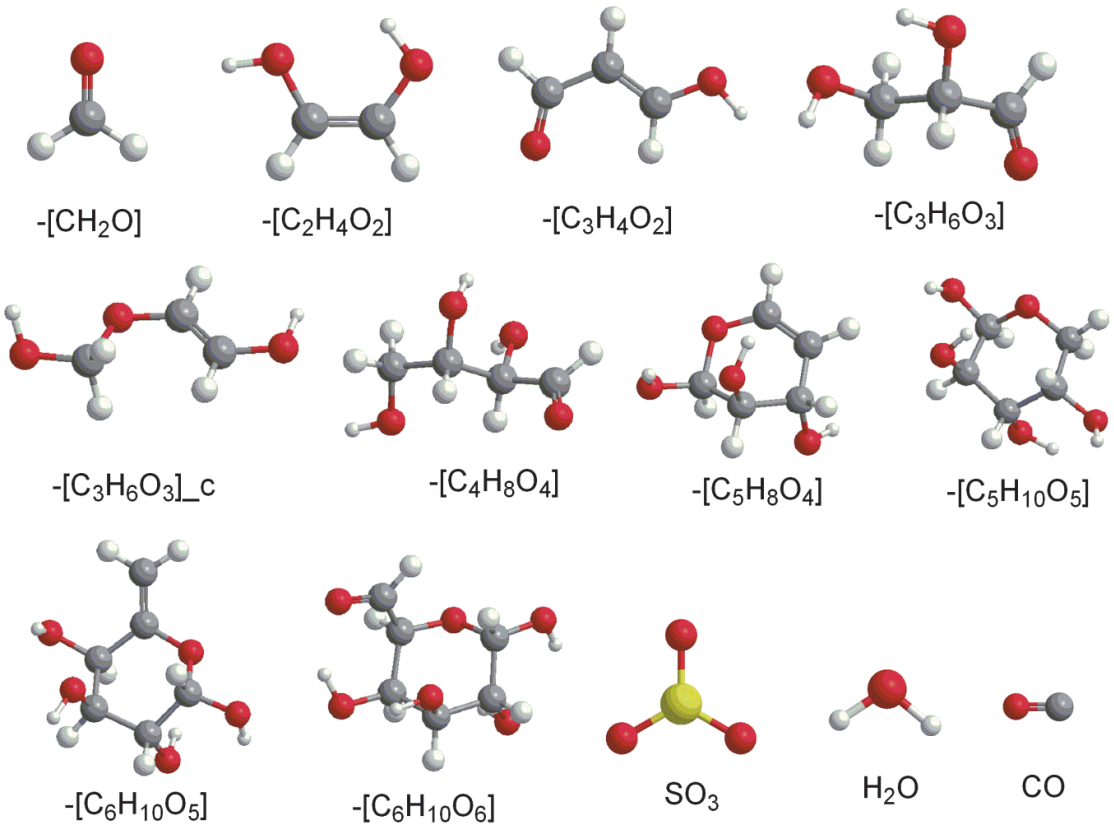
-[CH2O]
-[C2H4O2]
-[C3H4O2]
-[C3H6O3]
-[C3H6O3]_c
-[C4H8O4]
-[C5H8O4]
-[C5H10O5]
-[C6H10O5]
-[C6H10O6]
SO3
H2O
CO

Figure SI_B2

SI-C: Alternative mechanism for *m/z* 97

Scheme SI-C1: *m/z* 97 (97_C.mpg)

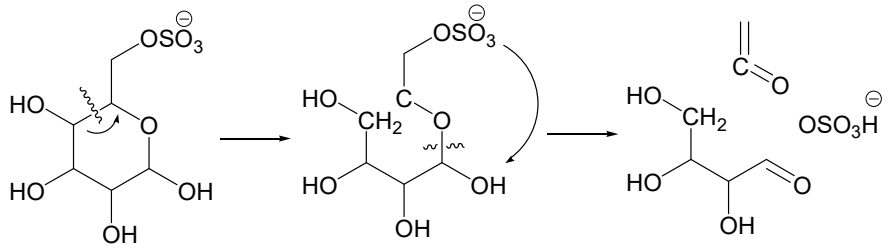

***m/z* 97**

$[HSO_4]^-$

Scheme SI-C2: *m/z* 97 (97_D.mpg)

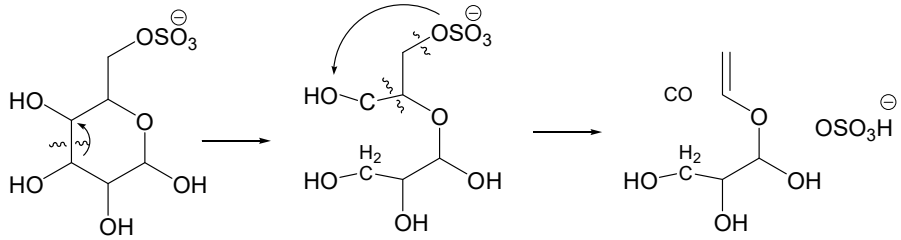

***m/z* 97**

$[HSO_4]^-$

SI-D: Fragmentation pathways for non-observed experimentally ions

Scheme SI-D1-[$C_3H_6O_4$] loss (*m/z* 213)

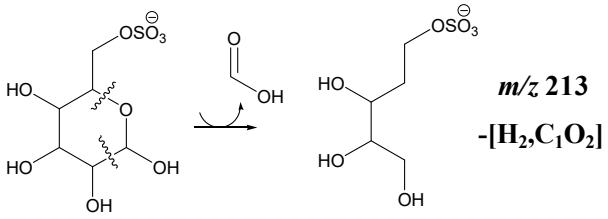

Figure SI-D1: Dissociation mechanism for formation of *m/z* 213

Scheme SI-D2-[$C_3H_6O_4$] loss (*m/z* 153)

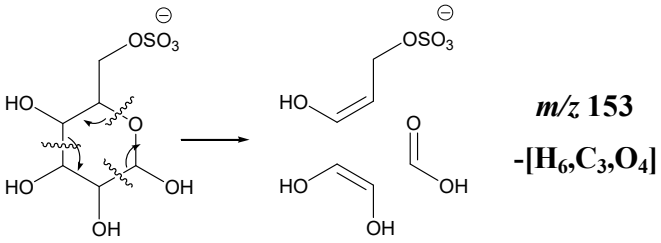

Figure SI-D2: Dissociation mechanism for formation of *m/z* 153

Scheme SI-D3-[H_2CO/SO_3] loss (*m/z* 149)

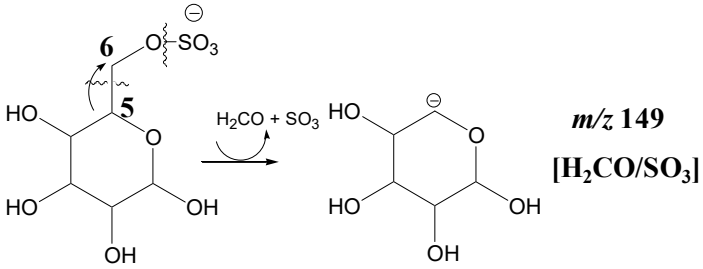

Figure SI-D3: Dissociation mechanism for formation of *m/z* 149

Scheme SI-D4-[$H_2CO/SO_3/H_2O$] loss (*m/z* 131)

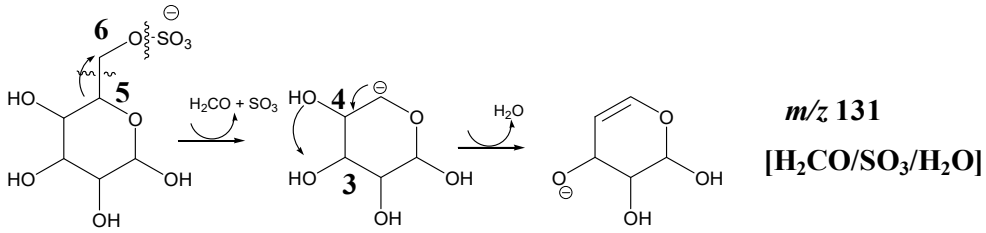

Figure SI-D4: Dissociation mechanism for the formation of the *m/z* 131 ion

Scheme SI-D5-[$H_2CO/SO_3/CO$] loss (*m/z* 121)

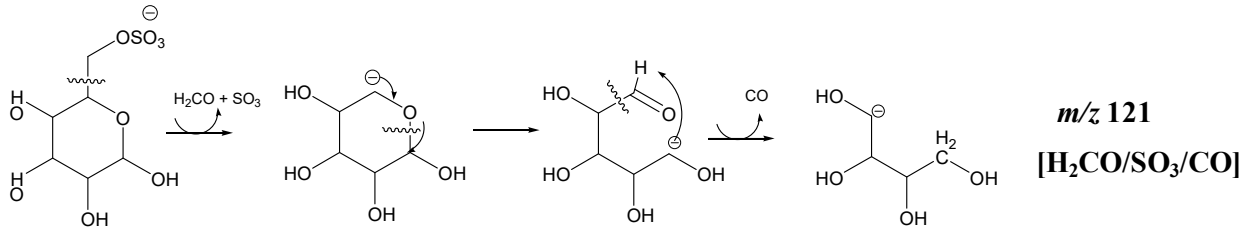

Figure SI-D5: Dissociation mechanism for formation of *m/z* 121

Scheme SI-D6-[$C_5H_{10}O_5$] loss (*m/z* 109)

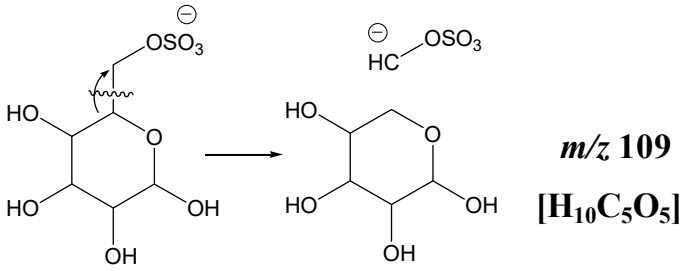

Figure SI-D6: Dissociation mechanism for formation of *m/z* 109

Scheme SI-D7-[$C_3H_4O_2/SO_3$] loss (*m/z* 107)

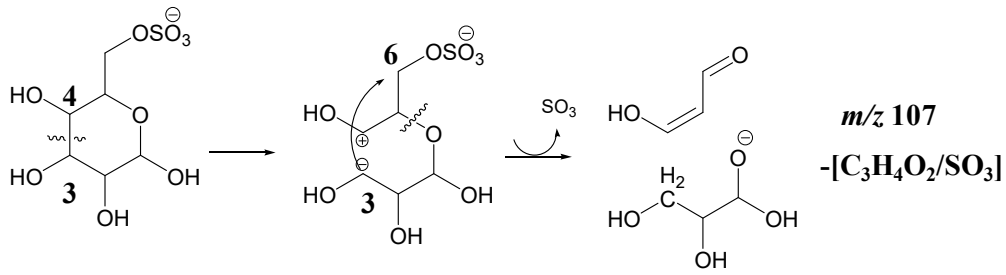

Scheme 7: Dissociation mechanism for formation of *m/z* 107

Scheme SI-D8-[$C_5H_{10}O_6$] loss (*m/z* 93)

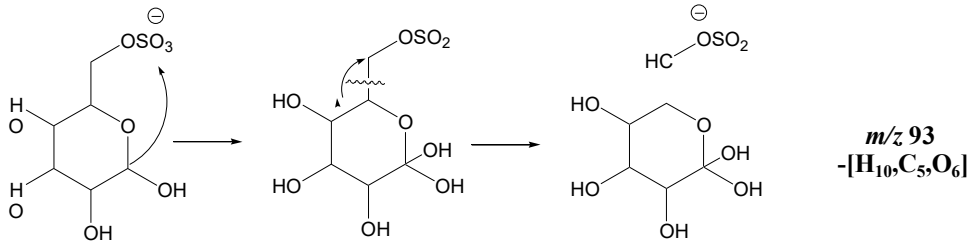

Figure SI-D8: Dissociation mechanism for formation of *m/z* 93

Scheme SI-D9-Formation of m/z 81 [HSO3]-

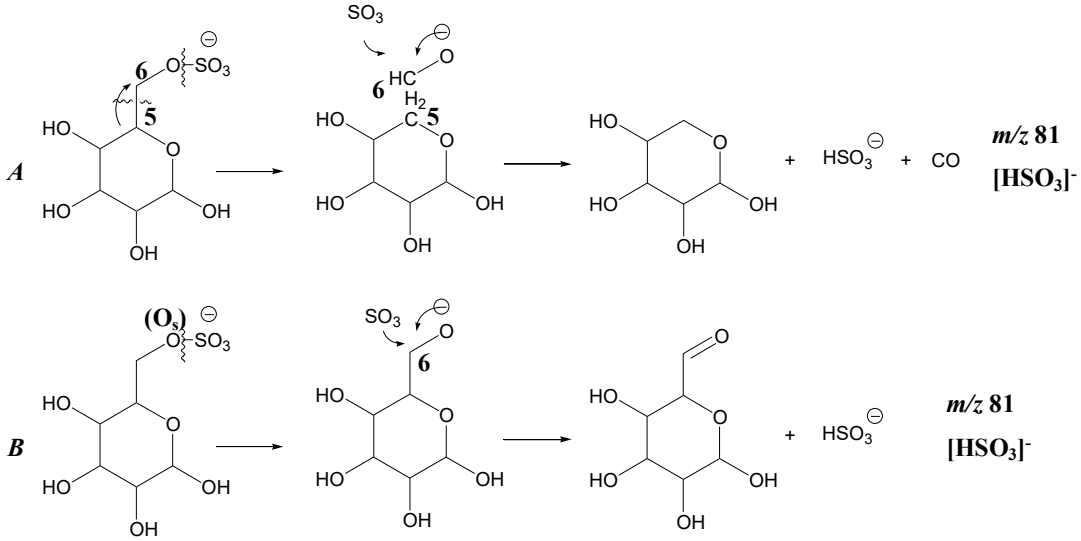

Figure SI-D9: Dissociation mechanisms for the formation of $[HSO_3]^-$ (*m/z* 81)).

Scheme SI-D10-[$C_4H_8O_3/SO_3$] loss (*m/z* 75)

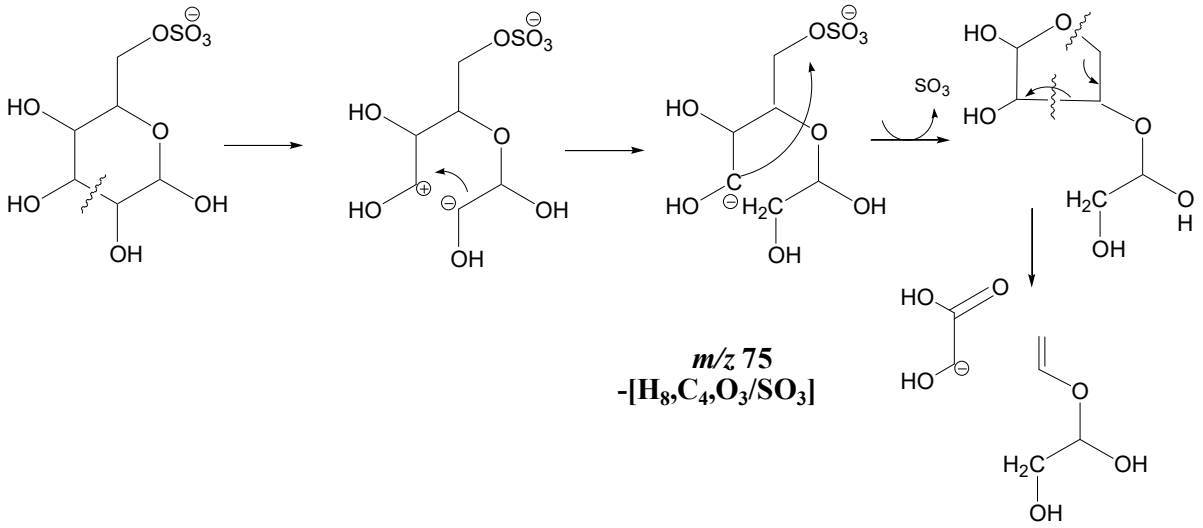

Figure SI-D10: Dissociation mechanism for formation of *m/z* 75

Scheme SI-D11-[$C_4H_6O_3/SO_3$] loss (*m/z* 74)

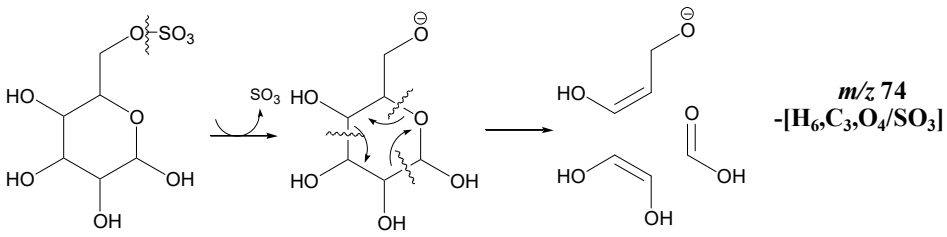

Figure SI-D11: Dissociation mechanism for formation of *m/z* 74

Scheme SI-D12 -[$C_3H_6O_3/SO_3/H_2O$]; formation of *m/z* 71

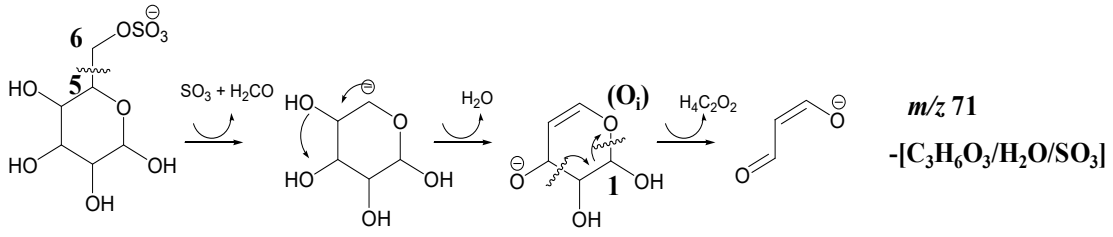

Figure SI-D12: Dissociation mechanism for the formation of *m/z* 71

Scheme SI-D13-[$C_4H_6O_3/SO_3$] loss (*m/z* 57)

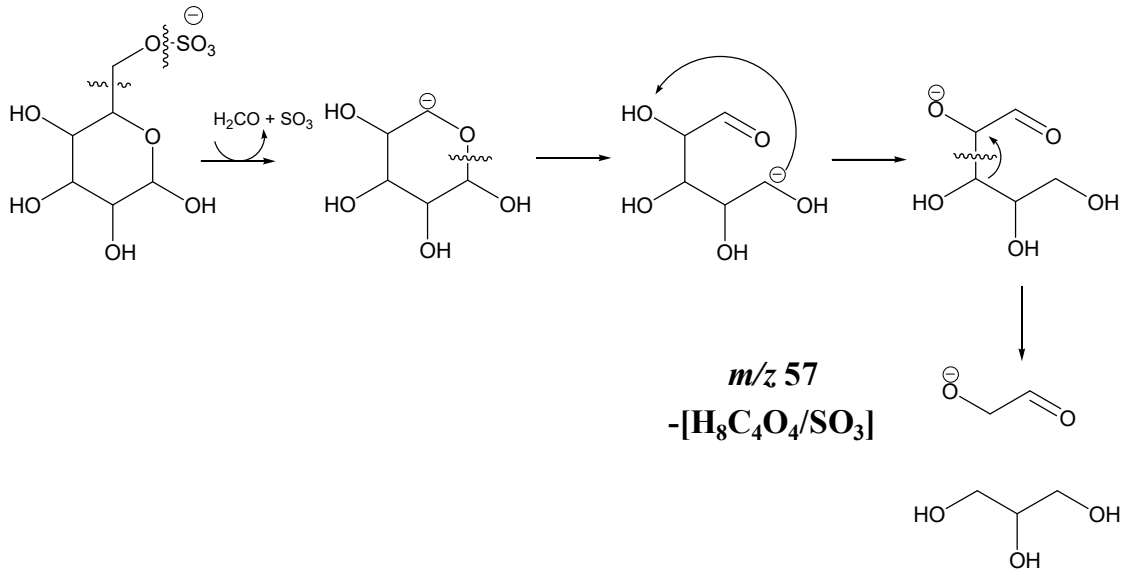

Figure SI-D13: Dissociation mechanism for formation of *m/z* 57

SI-E Vibrational and rotational energy of Gal-6S

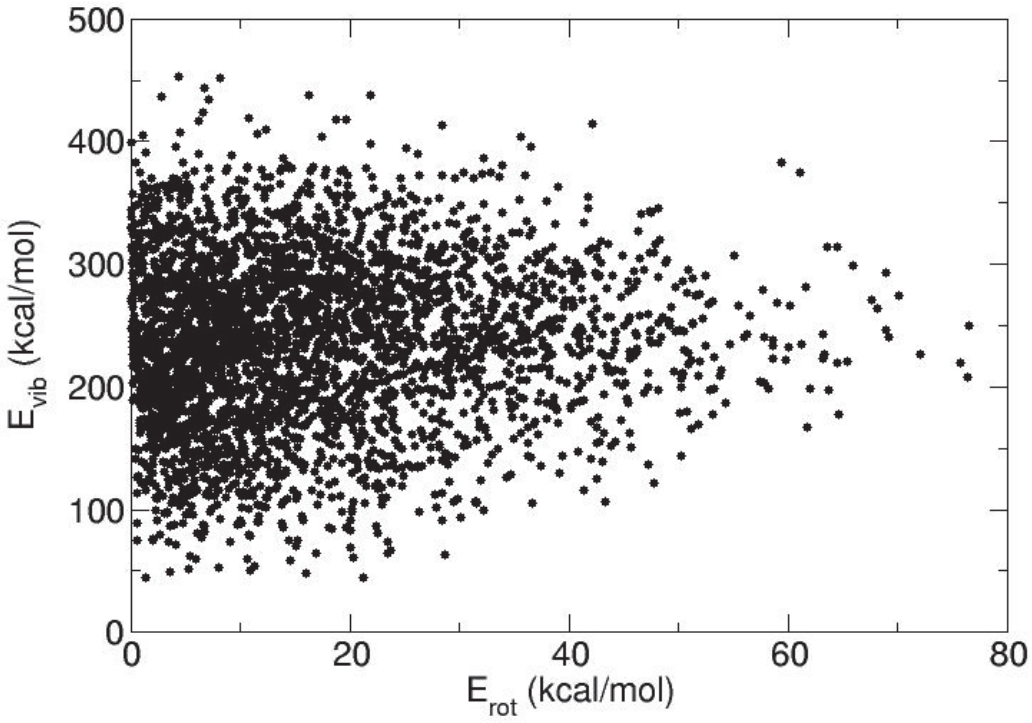

Figure SI-E: Vibrational and rotational energy of Gal-6S after collision with Ar as obtained by chemical dynamics simulations.